Searching for Beyond the Standard Model Physics with Photon Final States

by

Noah Steinberg

A dissertation submitted in partial fulfillment
of the requirements for the degree of
Doctor of Philosophy
(Physics)
in the University of Michigan
2021

Doctoral Committee:

Professor James Wells, Chair
Professor Ratindranath Akhoury
Professor Dante Amidei
Professor Aaron Pierce
Professor Laura Reustche

“The universe is a big place, perhaps the biggest.” — Kurt Vonnegut

Noah Steinberg

nastein@umich.edu

ORCID ID: 0000-0003-0427-4888

Acknowledgements

It is difficult to include every person who has ever helped me get to where I am today, it truly takes a village. First I would like to thank James Wells, who took me on as a new theory student in the beginning of what would be my third year as a graduate student. James is a remarkable scientist with a tremendous amount of wisdom that he has shared with me over the past three years. He has always encouraged me to develop my own set of ideas and taught me how to approach problems in a thoughtful and fruitful way. I would also like to thank Aaron Pierce, Henriette Elvang, Ratindranath Akhoury, and Wolfgang Lorenzon for their years of thoughtful mentorship and teaching

Switching from experimental to theoretical particle physics was no easy task, and without the kindness, encouragement, and friendship from my fellow theory graduate students, I would not be where I am today. Special dedication goes to Callum, Brian, and Shruti who through many pots of coffee and tea, challenged me intellectually and taught me an immense amount. They say you are the sum of the five people you spend the most time around, and I have become not only a better physicist, but a better person through my friendship with each of them.

Finally, I would never be where I am today without the help from my loving family. My parents, Gretchen and Mitch, have encouraged me on this journey since I was a young school child. They have made me into the thoughtful, caring, and ambitious person that I am today through their example. My last thanks goes to my partner Lucia, who has encouraged me, given me confidence, and taught me to appreciate my world and all that is out there. Words cannot describe how our journey has affected me, but I know that our world will continue to be exciting and I cannot wait to see what the future holds.

TABLE OF CONTENTS

List of Figures

FIGURE

List of Tables

TABLE

List of Appendices

APPENDIX

Abstract

The Standard Model, while remarkably successful at predicting phenomena down to length scales of $10^{-17}\,\mathrm{cm}$, is an incomplete theory, failing to account for several experimentally observed phenomena. The search for new physics which accounts for these observations, i.e. extending the Standard Model, is among the most important problems in particle physics today. Extensions of the Standard Model including singlet scalars or Axion-Like Particles (ALPs) are highly motivated due to their simplicity and abundance across the landscape of Beyond the Standard Model theories. In this thesis we have investigated the phenomenology of these generic models in several manifestations and developed novel search strategies for current and future experiments. At the Large Hadron Collider (LHC), a Higgs boson coupled to a light singlet scalar which decays primarily to photons can lead to a complicated final state involving overlapping photons. Developing observables sensitive to these collimated final states can vastly increase the sensitivity of the LHC to these exotic Higgs decays. Additionally I have shown that the future International Linear Collider (ILC) is sensitive to very weakly coupled ALPs across a wide range of masses. The ILC-GigaZ mode will produce 10^9 Z bosons allowing for a search for light ALPS via the rare $Z \to a\gamma \to \gamma\gamma\gamma$ decay mode, while using the almost real photons produced from incoming e^+e^- pairs in photon collisions at the ILC250 or ILC500 run modes at high energies will probe much heavier ALPs up to masses of 150(300) GeV.

Chapter 1

Introduction

1.1 Introduction to the Standard Model of Particle Physics

The natural world seems to obey powerful organizing principles whose low energy behavior is described by a quantum field theory (QFT). The Standard Model of particle physics [9] is a particular QFT that through almost a century of experimental and theoretical effort has been developed that describes our Universe. It is a gauge theory with gauge groups $SU(3)_c$ (color) and $SU(2)_L$ (weak isospin)$\times U(1)_Y$ (hypercharge) which is spontaneously broken down to $SU(3)_c$ and $U(1)_{EM}$ (electromagnetism) by a fundamental scalar, the Higgs boson [10], discovered at last in 2012 [11, 12].

The particle content of the standard model consists of matter particles - quarks and leptons - gauge bosons, and one fundamental scalar. Their representations under the standard model gauge groups are listed below in Table 1.1. Here we define the generators of $U(1)_Y$ so that the relationship between the conserved electric charge, Q, and the weak hypercharge is given by

$$Y_W := Q - T_3, \tag{1.1.1}$$

where T_3 is the third generator of $SU(2)_L$.

$G^A (A = 1, ..., 8)$, $W^a (a = 1, 2, 3)$, B are the spin-1 gauge bosons of $SU(3)_c$, $SU(2)_L$, $U(1)_Y$ respectively and we organize each fermion (q, l, u, d, e) into a three component column vector labeling the three generations. The Lagrangian of the Standard Model is given by the writing down all renormalizable, gauge invariant operators with minimal coupling between the matter particles and gauge fields. It is given by

$$\begin{aligned}\mathcal{L}_{SM} = &-\frac{1}{4}G^A_{\mu\nu}G^{A\mu\nu} - \frac{1}{4}W^a_{\mu\nu}W^{a\mu\nu} - \frac{1}{4}B_{\mu\nu}B^{\mu\nu} + |D_\mu\Phi|^2 - m^2_\Phi |\Phi|^2 - \lambda |\Phi|^4 \\ &+ \sum_{f\in q,l,u,d,e} i\bar{f}\gamma^\mu D_\mu f - [(\bar{u}y^\dagger_u q_\beta \varepsilon^{\alpha\beta} + \bar{q}^\alpha y_d d + \bar{l}^\alpha y_e e)\Phi_\alpha + \text{h.c.}].\end{aligned} \tag{1.1.2}$$

Table 1.1: Particle content of the Standard Model with representations under each gauge group

Field	$(SU(3)_c, SU(2)_L, U(1)_Y)$
$q_i = (u_L, d_L)_i$	$(\mathbf{3}, \mathbf{2}, \frac{1}{6})$
$l_i = (\nu, e_L)_i$	$(\mathbf{1}, \mathbf{2}, -\frac{1}{2})$
u_{Ri}	$(\mathbf{3}, \mathbf{1}, \frac{2}{3})$
d_{Ri}	$(\mathbf{3}, \mathbf{1}, \frac{-1}{3})$
e_{Ri}	$(\mathbf{1}, \mathbf{1}, -1)$
Φ	$(\mathbf{1}, \mathbf{2}, 1/2)$
G^a	$(\mathbf{8}, \mathbf{1}, 0)$
W^a	$(\mathbf{1}, \mathbf{3}, 0)$
B	$(\mathbf{1}, \mathbf{1}, 0)$

Here we define our covariant derivative which couples fermions and scalars to the gauge fields to be

$$D_\mu = \partial_\mu - ig_s T^A G^A_\mu - igt^a W^a_\mu - ig' Y B_\mu, \tag{1.1.3}$$

where g_s, g, g' are the coupling constants of $SU(3)_c, SU(2)_L, U(1)_Y$ respectively, and T^A are the generators of SU(3), t^a those of $SU(2)_L$, and Y labels the hypercharge of a given field.

Each SM fermion has a Yukawa coupling, y_u, y_d, y_e to the Higgs field Φ, which also couples left handed and right handed fermions together. These Yukawa couplings are complex 3×3 matrices in generation space, and can each be diagonalized by performing unitary transformations on the u_L, d_L, u_R, d_R fields. After EW symmetry breaking, the current which couples to the W boson involves u_L and d_L fields. The change of basis used above to diagonalize the Yukawa couplings leads to an off diagonal coupling between the physical u_L and d_L fields. The CKM matrix, V_{CKM}, encodes this misalignment between the gauge and mass-eigenstates in the down quark sector and allows for flavor mixing and CP violation which typically appear in charge current interactions.

1.2 Electroweak Symmetry Breaking

If the gauge symmetry of the Electroweak (EW) sector ($SU(2)_L \times U(1)_Y$) was unbroken, this would lead to four massless gauge bosons, a long range weak nuclear force, and massless quarks and leptons, all of which are of course contradicted by experiment. If the SM is the correct low energy description of nature, EW symmetry must be spontaneously broken. In the Standard Model this is accomplished by the introduction of a scalar Higgs field, Φ, with a Mexican Hat potential as in Eq. (1.1.2). As depicted in Fig. 1.1, the minimum of this potential forces Φ to get a vacuum expectation value (vev) $v = \sqrt{-m^2_\Phi/\lambda} = 246\,\mathrm{GeV}$.

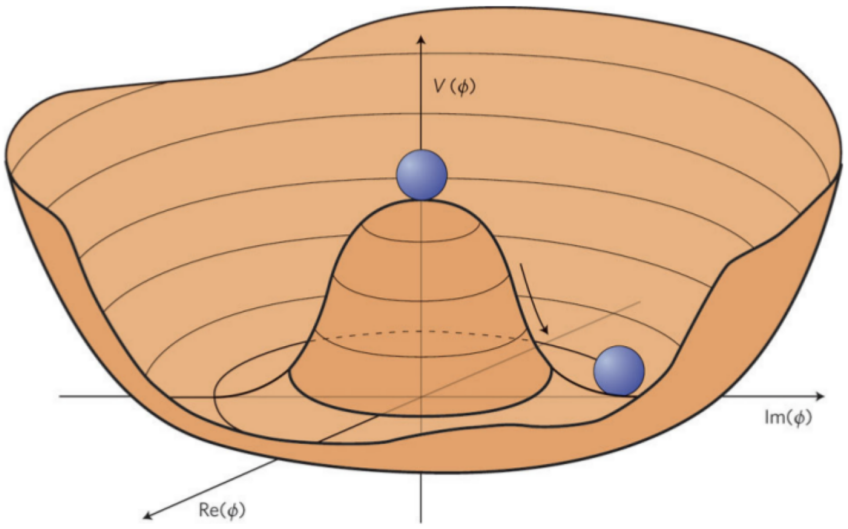

Figure 1.1: Potential energy of the Higgs field. The ground state of the potential gives the Higgs a vev, spontaneously breaking $SU(2)_L \times U(1)_Y$ down to $U(1)_{EM}$. Figure taken from [13]

Upon getting this vev, some of the gauge bosons obtain masses via the Higgs mechanism. This can be made concrete by transforming to Unitary Gauge. Parameterizing the complex doublet Φ in radial coordinates, $\Phi = (1/\sqrt{2})e^{i\frac{\pi^a}{v}t^a}(0, v+h)$ where t^a are the generators of $SU(2)$, one immediately sees that the goldstone bosons, π^a, can be removed from the theory via an $SU(2)\times U(1)$ gauge transformation, equivalent to setting $\pi^a = 0$. Taking the covariant derivative of Φ in this gauge, leads to terms quadratic in the gauge bosons.

$$\mathcal{L}_{\text{quadratic}} = \frac{1}{2}\frac{v^2}{4}[g^2(W_\mu^1)^2 + g^2(W_\mu^2)^2 + (-gW_\mu^3 + g^{'}B_\mu)^2]. \tag{1.2.1}$$

After diagonalizing the mass matrix of this system, we end up with three massive gauge bosons, and one massless gauge boson which we identify as the photon.

$$W_\mu^\pm = \frac{1}{\sqrt{2}}(W_\mu^1 \mp iW_\mu^2),\ Z_\mu = (c_W W_\mu^3 - s_W B_\mu),\ A_\mu = (s_W W_\mu^3 + c_W B_\mu), \tag{1.2.2}$$

where

$$c_W = \frac{g}{\sqrt{g^2+g^{'2}}} = \frac{e}{g^{'}},\ s_W = \frac{g^{'}}{\sqrt{g^2+g^{'2}}} = \frac{e}{g} \tag{1.2.3}$$

are the cosine and sine of the weak mixing angle respectively. The masses of the $W^\pm$ and the Z are given by $m_W = m_Z c_W = \frac{1}{2}gv$ at tree level.

Experimental verification of electroweak theory and the Higgs mechanism was accomplished over decades from the 1960s to the early 2010's beginning with the observation of weak neutral

currents in neutrino scattering at the Gargamelle bubble chambers [14]. This discovery indirectly verified the existence of the Z boson, and gave a prediction for the mass of the W. This motivated the construction of the Super proton-antiproton Synchrotron (SppS) at CERN, where in the 1980's the W and Z bosons were directly produced and observed through their decay products [15, 16].

The direct discovery of the massive electroweak gauge bosons lead to the LEP program, which verified the EW theory beyond tree level, establishing the SM as the quantum theory of the EW interactions. The final stage of the program was the discovery of the Higgs boson in 2012 at the ATLAS and CMS experiments [11, 12].

1.3 The Higgs Boson

The Higgs boson plays a fundamental role in the Standard Model as the trigger for electroweak symmetry breaking. In combination with being the only fundamental scalar of which we know, the Higgs boson represents an exciting opportunity to test the Standard model and discover new physics. Higgs physics is a rich and a mature field of study, currently be probed at the highest energies at the LHC with only $139\,\mathrm{fb}^{-1}$ of integrated luminosity. This is less than 5% of the total luminosity that the LHC will collect, and with increasing data the discovered Higgs boson will be put to the test. Does it couple to the masses of the fermions and vector bosons as a predicted? What is the nature of the Higgs self coupling which drives electroweak symmetry breaking and imprints itself on the stability of the vacuum at high energies? What is the role of the Higgs boson in unitarizing the SM at high energies?

Let us examine the last question. A Higgs-less SM violates unitarity at high energies in vector boson scattering. This is because at high energies the amplitude for the scattering of longitudinal gauge bosons $\mathcal{A}(V_L V_L \to V_L V_L)$ involves the longitudinal polarization vectors

$$\lim_{k\to\infty} \varepsilon_L^\mu(k) = k^\mu/m \tag{1.3.1}$$

which diverge with energy as the momentum of the gauge bosons is taken to infinity. Take $(W_L^+ W_L^- \to W_L^+ W_L^-)$ as an example.

One exemplary Feynman diagram (the contact interaction) for this process is depicted in Fig. 1.2. The sub-amplitude calculated from this diagram is

$$\begin{aligned}\mathcal{A}_{contact} = 4\sqrt{2}G_F m_W^2 \,(2(\epsilon_L^*(k_1)\epsilon_L(p_2))(\epsilon_L^*(k_2)\epsilon_L(p_1)) &- (\epsilon_L^*(k_1)\epsilon_L(p_1))(\epsilon_L^*(k_2)\epsilon_L(p_2)) \\ &- (\epsilon_L^*(k_1)\epsilon_L^*(k_2))(\epsilon_L(p_2)\epsilon_L(p_1)).\end{aligned} \tag{1.3.2}$$

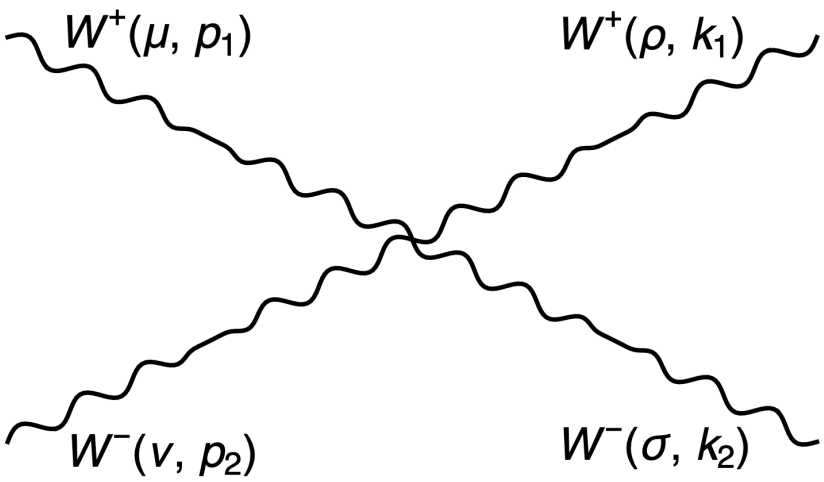

Figure 1.2: Feynman diagram for the contact interaction leading to $(W_L^+W_L^- \to W_L^+W_L^-)$. This sub-amplitude contributes an s^2 divergence.

Though this diagram by itself is not gauge invariant, it demonstrates the dangerous high energy behavior of the longitudinally polarized W's, rising with s^2 after using Eq. (1.3.1) for the polarization vectors. Gauge invariance mandates the introduction of amplitudes involving the exchange of Z bosons and photons, which fortunately softens the divergence of the Higgs-less amplitude. The full (Higgs-less) amplitude for this process is lengthy, but can be computed straightforwardly in Unitary gauge. Inserting the longitudinal polarization vectors and expanding in powers of s (the center of mass energy squared) gives an amplitude

$$\mathcal{A}_{Higgs-less} = \sqrt{2}sG_F\cos^2\left(\frac{\theta}{2}\right) + \frac{G_F\csc^2(\frac{\theta}{2})m_W^2(\sin^2(\theta)+4\cos(\theta)+8\sin^4(\frac{\theta}{2})\sin^2(\theta_W))}{\sqrt{2}\cos^2(\theta_W)} + \mathcal{O}\left(\frac{1}{s}\right). \tag{1.3.3}$$

The above amplitude linearly diverges with s, which signals a breakdown of unitarity and the theory. Much like how unitarity is violated in Fermi theory and restored by the massive vector bosons, the introduction of the Higgs cancels this last divergence and unitarizes the theory. In fact this behavior was used to bound the mass of the Higgs long before it was discovered [17]. The LHC has recently measured vector boson scattering (VBS) for the first time [18, 19] with over 5σ significance, and has been able to separate the different polarization contributions to this process in order to extract the contribution of longitudinally polarized vectors [20], but only has weak $< 3\sigma$ evidence for this process. In the future, the LHC hopes to measure longitudinal vector boson scattering with high precision, and probe the breakdown of unitarity in the SM [21]. This

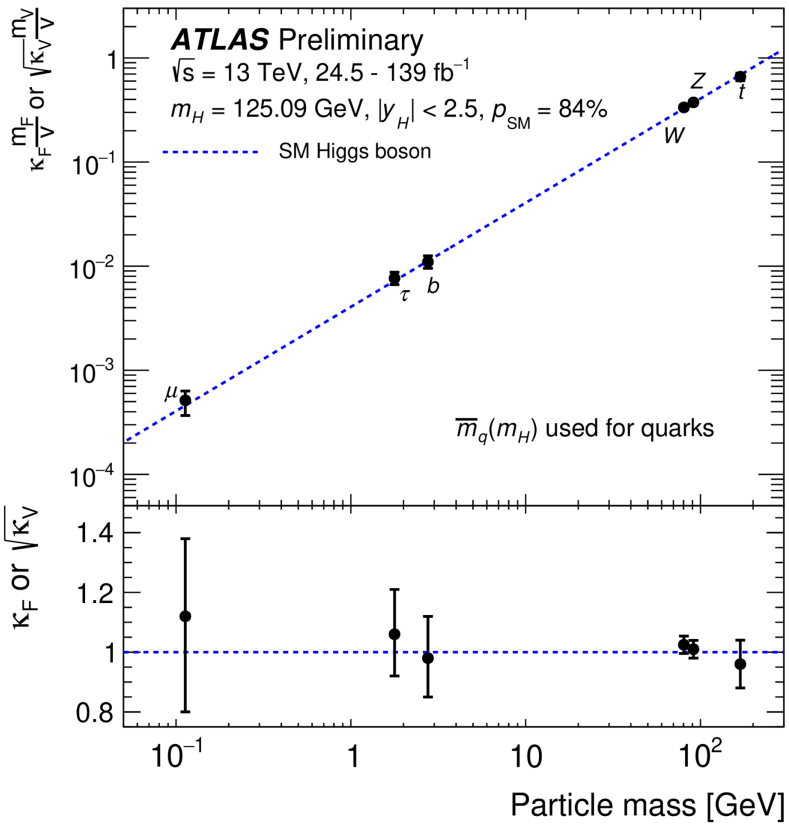

Figure 1.3: Coupling strength modifiers for fermions and weak gauge bosons as a function of mass. SM prediction is shown in dashed blue. Figure taken from [1]

is but one example of the overarching importance of the Higgs in the SM and makes it an exciting particle to study.

In the SM the tree level Higgs boson couplings to the SM particles are precisely determined in terms of their masses. Fig. 1.3 shows the Higgs coupling to standard model fermions and gauge bosons as a function of the mass of that particle vs the experimentally determined coupling strengths. Here one sees excellent agreement between the SM and experiment for the third generation fermions and heavy gauge bosons, where as for second generation fermions more data needs to be taken.

The Higgs boson also couples to the massless gluon and photon at the loop level through the virtual exchange of heavy fermions and gauge bosons. It is a remarkable fact that even though these tree level couplings do not exist, the main Higgs production mode at the LHC is via gluon-gluon fusion with a production cross section $10\times$ larger than the next largest mode [2], and the discovery of the Higgs was made via its decay to two photons. The importance of the above production and decay modes of the Higgs necessitates the calculation of the gluon-gluon fusion

(ggF) cross section and the diphoton decay mode to high orders of perturbation theory. Currently the ggF cross section is calculated at $\mathrm{N^3LO\,QCD + NLO\,EW}$ accuracy. This calculation can be done in an effective field theory framework where the top quark is integrated out and an effective Lagrangian where the Higgs couples directly to gluons is obtained as in Eq. (1.3.4)

$$\mathcal{L}_{\mathrm{TopEFT}} = -C_1 \frac{\alpha_s}{12\pi} \frac{h}{v} G^{A\mu\nu} G^A_{\mu\nu}. \tag{1.3.4}$$

In the above, C_1 is the Wilson coefficient obtained from integrating out the top quark and at leading order in α_s takes the value $C_1 = 1$. The coefficient of this effective operator can be obtained from the decoupling coefficient[1] of the strong coupling via a Higgs low energy theorem [22]. Currently this coefficient is actually known to $\mathrm{N^4LO}$ [23].

The Higgs boson discovery strategy used by the LHC was largely influenced by comparing background rates versus the various strengths of the Higgs boson decay modes into SM particles, i.e. the Higgs branching ratios. Higgs branching ratios to all SM particles are shown in Fig. 1.4. As can be seen in the figure, in the region between $120 - 130\,\mathrm{GeV}$ the dominant decay mode of the Higgs is to $b\bar{b}$ and WW^* with all other decay modes suppressed by at least an order of magnitude. Even though the branching ratio to photons is only $\mathcal{O}(10^{-3})$ this decay mode along with $h \to ZZ^* \to 4l$ was amongst the first to be discovered at the LHC due to the extremely clean final state and relatively low backgrounds.

Interestingly the Higgs branching ratio to invisible states is only very weakly constrained. In the SM the Higgs decays invisibly only through $H \to ZZ \to 4\nu$, with a branching fraction $B(h \to ZZ) \times B(Z \to \nu\bar{\nu}) \approx 10^{-3}$. Searches for $h \to \mathrm{inv}$ are pursued in the VBF, VH, and ggF mode where combined they give an upper limit of $B(h \to \mathrm{inv}) < 0.19$ at 95% CL [24]. This means that the Higgs could be decaying to invisible or undetected BSM states up to 20% of the time. It is extraordinary that a particle that we have been studying theoretically for 50 years and that plays such an essential role in the SM is so unconstrained.

1.4 The Need for Physics Beyond the Standard Model

Despite the success of the Standard Model defined in Sec. 1.1 , it is known that the SM is incomplete. This comes from myriad of experimental and theoretical results of which we will name a few.

[1]The decoupling coefficient in QCD relates the gauge coupling $\alpha_s = \frac{g_s^2}{4\pi}$ across quark mass thresholds, i.e. it relates the $\alpha_s^{(n_f=6)}$ with all quarks present in the theory to $\alpha_s^{(n_f=5)}$ with the top quark integrated out via. $\alpha_s^{(n_f=6)} = \zeta^2 \alpha_s^{(n_f=5)}$

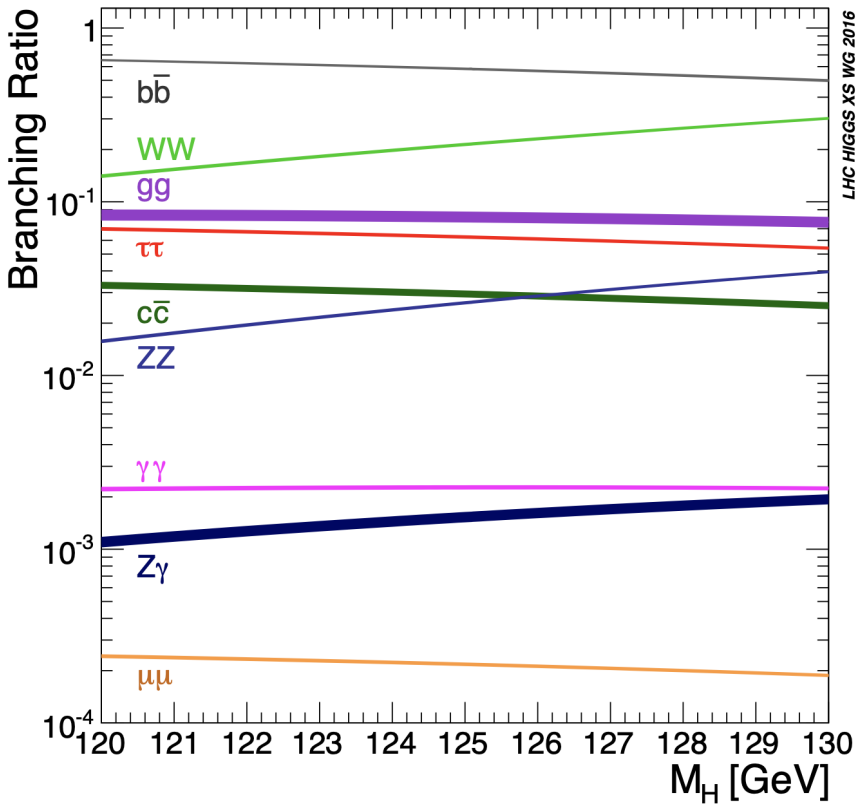

Figure 1.4: Higgs boson branching ratios and their uncertainties. Figure taken from [2].

- Experimental evidence across an array of cosmic and astrophysical distance scales shows that only 15% of the matter in the Universe is baryonic and interacts electromagnetically [25]. The other 85% of the matter is made up of an unknown substance dubbed Dark Matter. Viable candidates for dark matter span from masses of $10^{-22}\,\mathrm{eV}$ [26], set by the constraint $\lambda_{deBroglie} \approx 1\,\mathrm{kpc}$, to macroscopic masses of 10^4 solar masses [27], constrained by requiring that granular DM does not disrupt gravitationally bound systems. Weakly Interacting Massive Particles (WIMPs) are a particularly excellent candidate due to giving the correct relic density of Dark Matter with masses at or around the weak scale, though the parameter space allowed for WIMPs is quickly shrinking thanks to experiments like LUX, and Xenon1T [28]. Another viable candidate is the axion, which is a psuedo-nambu goldstone boson of PQ symmetry breaking [29]. Along with providing a viable Dark Matter candidate, axions also give a dynamical solution to the Strong CP problem, i.e. why is CP violating parameter $\bar{\Theta} \approx 0$ [30]? A last promising candidate is sterile neutrinos. A right handed neutrino N_R is absent in the SM, but if it is present it would give a viable DM candidate [31] as well as provide an explanation for neutrino masses.

- The matter-antimatter asymmetry of the universe can be summarized by the measured value of the baryon to entropy ratio $\eta = \frac{n_B}{s} = \frac{n-n_{\bar{b}}}{s} \approx 6.1 \times 10^{-10}$. The origin of this matter-antimatter asymmetry in the universe is currently unknown and a solution cannot be found in the Standard Model alone. One of the Sakharov conditions for baryogenesis (which is a direct consequence of this asymmetry) is that there be CP violation in the early universe [32]. In the Standard model CP violation is present in the quark sector via the CKM matrix. This CP violation is too small to account for the matter-antimatter asymmetry [33], new physics must be present to generate the necessary CP violation. Many models of new physics have new sources of CP violation including the Minimal Supersymmetric Standard Model (MSSM), Two-Higgs Doublet models, and a host of others. Any new CP violation must respect the constraints from measurements in the K^0 and B meson systems as well as searches for electric dipole moments (EDMs) [34,35]. Neutrinos may provide the necessary CP violation via the PMNS mixing matrix which contains one CP violating phase and 2 majorana phases. Neutrino oscillation experiments currently favor maximal CP violation [36] though more data needs to be taken.

- The discovery of neutrino oscillations [37] over the past 30 years implies that at least two of the three neutrino species are massive, yet the SM contains no mechanism for neutrinos to obtain a mass. Thus neutrino masses $guarantee$ the presence of BSM physics. There are numerous neutrino mass models in the literature, but the most common version is some modification of the standard seesaw mechanism [38]. In the seesaw mechanism, one introduces 3 right handed neutrinos N_R with yukawa coupling to the Higgs of the form $y_\nu \bar{L} H N_R$. Additionally, the N_R as gauge singlets may enjoy Majorana masses $M_R N_R^T C^{-1} N_R$ with M_R unconstrained. For $M_R \gg y_\nu v$, diagonalizing the neutrino mass matrix leads to light neutrino masses of order $y_\nu v / M_R$. Thus order one yukawa couplings along with $M_R \approx 10^{12} GeV$ could explain the lightness of the left handed neutrinos.

- The electro-weak scale characterized by $m_{EW} = v$ is 16 orders of magnitude smaller than M_{pl}, which sets the strength of gravitational interactions. This disparity in scales, known as the Hierarchy Problem, is among the most theoretically concerning and interesting problems in theoretical particle physics as it is directly entangled with the notion of naturalness. Many concrete statements about naturalness exist in the literature, but they can be summarized by the idea that a theory is natural if and only if the IR parameters of the theory are insensitive to the UV physics of the theory. The measured Higgs mass of $125\,\mathrm{GeV}$ is a danger to this notion of naturalness. To see this, consider adding a cut off to the SM, Λ, which denotes the point at which new physics must appear. Quantum corrections to the Higgs mass due to the top quark are cut off at Λ so that the 1-loop correction to the physical Higgs mass is given by $m_h^2 = m_{bare}^2 + \frac{y_t^2 \Lambda^2}{16\pi^2}$. Here the hierarchy problem rears its head with the famous quadratic divergence in the Higgs mass. If Λ is near M_{Pl} then

this requires a tremendously precise cancellation or "tuning" to give the measured Higgs mass of $125\,\mathrm{GeV}$. To reduce this tuning, Λ should be at or around the TeV scale. But this need for a low cutoff is in direct conflict with constraints on the scale of new physics from other sectors. New particles contributing to neutral meson mixing would far exceed the SM contribution unless these new particles have masses greater than about $10^3\,\mathrm{TeV}$ [39].

Even in the absence of a cut off, the Higgs mass is unsafe from quantum corrections. Taking the $SU(5)$ Grand Unified Theory (GUT) as an example, the SM Higgs in the $\bar{\mathbf{5}}$, couples to the $SU(5)$ breaking scalar $\mathbf{24}$. At one loop, the quartic coupling $\lambda\bar{\mathbf{5}}\mathbf{24}^2\mathbf{5}$ receives a correction proportional to g_U^4 [40], where g_U is the unified gauge coupling. After EW symmetry breaking this quartic coupling gives a mass to the Higgs proportional to

$$\lambda < \mathbf{24} >= \lambda M_U, \tag{1.4.1}$$

where M_U is the unification scale taken to be near $10^{16}\,\mathrm{GeV}$. Taking $m_h = 125\,\mathrm{GeV}$ requires a precise cancellation between the $\lambda(M_U)$ and the one loop correction described above. In the most general sense, scalar masses tend to be driven to the highest scales in the theory. Supersymmetry offers one solution to the Hierarchy problem as the Higgs inherits the chiral symmetry of its super-partner, which protects its mass from large radiative corrections. Again this solution is in tension with direct experimental constraints from production [41] and indirect precision constraints, as low scale supersymmetry gives large contributions to flavor and CP violating observables. This requires that scalar super-partner masses be large or that the structure of the MSSM soft terms be very special [42].

1.5 Parameterizing new physics - Simple Extensions of the SM

The last section highlighted some of the glaring problems which require solutions outside of the Standard Model. To supplement the standard model requires the addition of new states and or symmetries to the theory. This leads to an innumerable collection of BSM theories which must not only predict new phenomena/explain the unanswered questions in Sec. 1.4 and more, but also evade all current experimental constraints. This is a powerful problem to overcome for any proposed model, as the experimental constraints on rare SM processes push the scales at which new physics may arise to higher and higher energies. In many models this often requires fine tunings of parameters or the inclusion of further states and pushes the theory to corners of parameter space that are harder to motivate than the problems which the theory was originally set out to solve.

This motivates the exploration of simple, generic extensions of the Standard Model, which can serve as benchmarks and be re-interpreted later in the context of more complicated or complete

models. What are the most generic/simple extensions of the Standard Model? Naturally, we turn to scalar/pseudo-scalar states as these new states cannot be anomalous and can easily be concatanated with SM operators in a renormalizable or non-renormalizable fashion. Additionally, we make the assumption that these states are singlets under the SM gauge groups. This is motivated by the genericness of hidden sectors, i.e. those not charged under G_{SM}, in UV complete theories like string theory. These hidden sectors may also provide excellent dark matter candidates. Under these conditions, we arrive at extending the standard model via scalar and pseudo-scalar singlets.

Scalar singlet extensions are unique in their simplicity but diverse in their phenomenology. Consider the following Z_2 symmetric Lagrangian

$$\mathcal{L}_{Singlet} = \mathcal{L}_{SM} + \frac{1}{2}(\partial_\mu \phi)^2 - m_\phi^2 \phi^2 - \lambda_\phi \phi^4 - \lambda_{\Phi\phi} \Phi^\dagger \Phi \phi^2 \tag{1.5.1}$$

If ϕ gets a vev, v_ϕ, then this leads to a mixing between the neutral non-goldstone part of Φ and ϕ. The resulting physical states h and H couple to all SM particles in the same way as the SM Higgs, but with reduced coupling strength. This simple model contains three physical parameters which are undetermined: the mixing angle α between the observed 125 GeV Higgs and the new state, the new heavy Higgs mass m_H[2], and $\tan\beta = v_\phi/v$. These physical parameters can at tree level be expressed in terms of the Lagrangian parameters as follows:

$$\begin{aligned} \lambda &= \frac{m_h^2}{2v^2}\cos^2\alpha + \frac{m_H^2}{2v^2}\sin^2\alpha \\ \lambda_\phi &= \frac{m_h^2}{2v_\phi^2}\sin^2\alpha + \frac{m_H^2}{2v_\phi^2}\cos^2\alpha \\ \lambda_{\Phi\phi} &= \frac{(m_H^2 - m_h^2)}{2vv_\phi}\sin 2\alpha, \end{aligned} \tag{1.5.2}$$

where λ is the quartic coupling for Φ. As we know that the 125 GeV Higgs observed at the LHC is SM-like, $\sin\alpha$ must be small so as to not disturb the overall 125 GeV Higgs coupling strength. More powerful constraints on this model come from radiative corrections to the mass of the W. Matching the effective Fermi theory of muon decay to the full SM gives a relationship between the W mass and the SM quantity Δr,

$$m_W^2\left(1 - \frac{m_W^2}{m_Z^2}\right) = \frac{\pi\alpha_{em}}{\sqrt{2}G_F}(1 + \Delta r) \tag{1.5.3}$$

Using m_Z and G_F as experimental inputs and computing Δr gives a prediction for m_W. One of the key components of Δr is the ρ parameter [43]. In the SM, the ρ parameter measures the ratio of the neutral current and charged current couplings of four-fermion processes, $\rho = G_{NC}/G_{CC}$. At low energies the LO value of G_{NC} and G_{CC} are computed by setting the momentum transfer

[2]Here we assume that the 125 GeV Higgs observed is the lighter of the two mass eigenstates

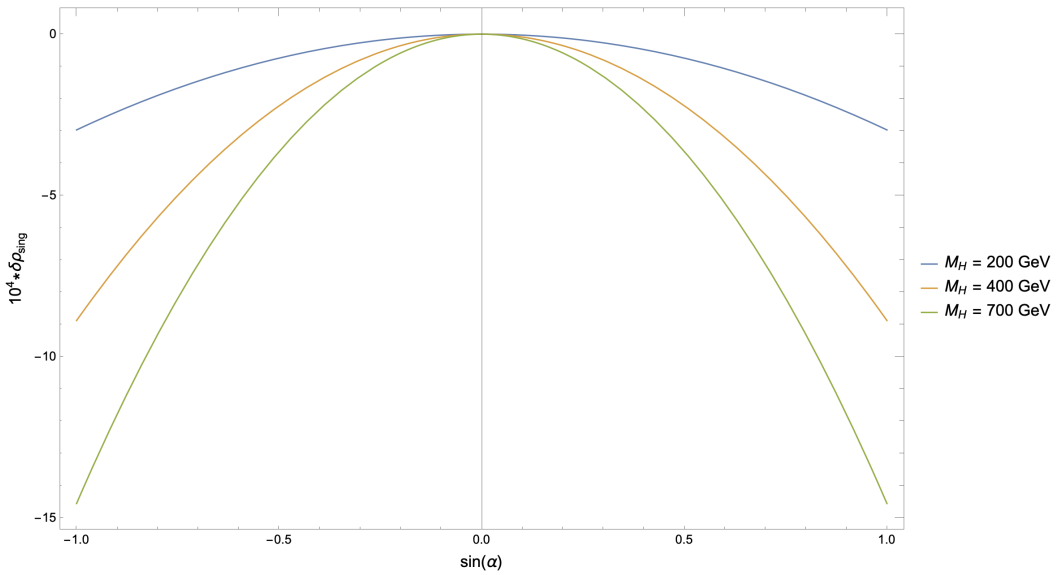

Figure 1.5: Singlet contributions to $\delta\rho$ as a function of $\sin\alpha$ at mixed heavy Higgs masses of 200, 400, and 700 GeV. $\delta\rho$ gives the main contribution of the singlet model to the Δr parameter or equivalantly the shift in the W boson mass.

to 0 in the propagators of the W and Z. Thus at tree level in the SM, ρ is given by

$$\frac{G_{NC}}{G_{CC}} = \frac{e^2/8s_W^2c_W^2m_Z^2}{e^2/8s_W^2m_W^2} = \frac{m_W^2}{c_W^2m_Z^2} = 1. \tag{1.5.4}$$

At higher orders, the calculation of the low energy couplings leads to a deviation $\delta\rho$,

$$\rho = \frac{1}{1-\delta\rho} \tag{1.5.5}$$

where $\delta\rho$ can be calculated in a loop order expansion. The deviation of $\delta\rho$ from 0 signifies custodial symmetry breaking, and is an important ingredient for precision electroweak observables. At one loop $\delta\rho$ is given by

$$\delta\rho = \frac{\Sigma_Z(0)}{m_Z^2} - \frac{\Sigma_W(0)}{m_W^2} \tag{1.5.6}$$

Here $\Sigma_V(0)$ $(V = W, Z)$, is the vector boson self energy at 0 momentum transfer. In the SM the main contribution to $\delta\rho \neq 0$ is the splitting of the top-bottom mass, but the singlet extension gives non negligible contributions to $\delta\rho$ as well. Below we plot the new singlet contribution to $\delta\rho$ at one loop as a function of $\sin\alpha$ at fixed values of m_H. Fig. 1.5 highlights the increasingly negative contribution of the singlet model as $|\sin\alpha|$ and m_H increase. The experimental precision on M_W then puts powerful constraints on the singlet model, $|\sin\alpha| < 0.3$ for $m_H > 250GeV$ [44] compared to $|\sin\alpha| < 0.5$ from the overall Higgs signal rate.

If the role of the heavy and light Higgs in this model are switched (i.e. the 125 GeV Higgs is the state H), and the new scalar mass eigenstate has a mass $m_h < m_H/2$, then this opens up a new decay channel for the 125 GeV Higgs.

Depending on the final states into which h can decay this may lead to $H \to \text{invisible}$ or to SM final states. Extending the above singlet model by coupling the scalar singlet to photons in a non-renormalizable way opens the possibility to detect the couplings of the 125 GeV Higgs to these new states through their decay into photons, i.e. the decay chain $H \to hh \to 4\gamma$. This decay chain can be especially difficult to detect when the mass of the light scalar $\mathcal{O}(\text{GeV})$ as the final state photons can be highly collimated, leading to a difficult to detect final state. With the Higgs being a focal point of study in the high energy world, and it's branching ratios still not tightly constrained, these rare BSM decay modes become even more important to search for. We explore the phenomenology of this extension in Chapter 1.

Pseudo-scalar singlets or Axion-Like Particles are similar in simplicity to the scalar case, but often derive from a different set of UV models. ALPs often arise from spontaneous symmetry breaking where they are pseudo-nambu goldstone bosons (PNGB). Examples of ALPs can be found in some composite Higgs models, or in majaron, or familion models. Perhaps the most famous pseudo-scalar singlet is the axion, which as mentioned before is both a Dark Matter candidate and a possible solution to the strong CP problem.

The original axion model relies on a new $U(1)_{PQ}$ symmetry which is spontaneously broken by the vev of a complex scalar field

$$< \phi >= (f_a/\sqrt{2})e^{ia/f_a}. \tag{1.5.7}$$

The Goldstone boson, a, is the axion. Extra quark fields charged under the PQ symmetry and $SU(3)_c$ make the PQ symmetry anomalous so that the generated anomaly term corresponding to a chiral rotation by a/f_a leads to an additional term in the action

$$\int d^4x \frac{a\alpha_s}{8\pi^2 f_a} G^A_{\mu\nu}\tilde{G}^{A\mu\nu}. \tag{1.5.8}$$

with $G^{A\mu\nu} = \frac{\epsilon^{\mu\nu\rho\sigma}}{2} G^A_{\rho\sigma}$ being the dual field strength tensor. Thus the total CP violating term is given by

$$(\frac{a}{f_a} - \bar{\Theta})\frac{\alpha_s}{8\pi} G^A_{\mu\nu}\tilde{G}^{A\mu\nu}, \tag{1.5.9}$$

where $\bar{\Theta}$ is the effective Θ parameter after absorbing the phases which come from diagonalizing the quark mass matrix. Finally, instantonic field configurations generate a potential for the axion whose minimum is naturally CP conserving, i.e. the value of the field is driven to $\bar{\Theta} f_a$. This is the axion solution to the strong CP problem. This first axion model predicts an axion mass and

couplings, dictated solely by f_a, which can be computed in chiral perturbation theory. The axion mass at NNLO is calculated as [45]

$$m_a = 5.691(51) \left(\frac{10^9 \,\mathrm{GeV}}{f_a} \right) \,\mathrm{meV}. \tag{1.5.10}$$

Plugging in $f_a = \mathcal{O}(10^2)\,\mathrm{GeV}$, which puts the scale of PQ breaking at the EW scale, gives an axion mass in the KeV range. Though some model dependencies remain in the axion couplings, experimental searches for the original QCD Axion in reactor, beam-dump, and meson decay experiments have shown no excesses, ruling out this simple model with a low PQ breaking scale [46]. This realization lead to the growth of "invisible axion" models [47, 48], i.e. those where $f_a \gg v$. In these models, additional scalars or heavy quarks are introduced which result in small axion masses and extremely tiny ALP-SM couplings, evading most experimental constraints. A further generalization leads to Axion-Like Particle models whose masses and couplings are not necessarily related to each other. In Chapters 2 and 3 we explore one such Axion-Like Particle model where the ALP is coupled to the SM hypercharge through a higher dimension operator. We find a rich spectrum of experimental signatures which can be probed at the future ILC experiment.

1.6 Outline of this dissertation

This dissertation consists of three main chapters, each studying search strategies for BSM physics involving additional scalar/pseudo-scalar particles. The first chapter focuses on searches involving the Higgs boson decaying to light scalar while the second and third are a searches for Axion-Like Particles (ALPs) at the future ILC experiment. An outline of each chapter is given below:

1.6.1 Chapter 2: Higgs boson decays into narrow di-photon jets and their search strategies at the Large Hadron Collider

The Higgs branching ratio to invisible or exotic states is poorly constrained by current experimental measurement. Higgs decays to light scalar singlets which also couple to photons represent a challenging BSM scenario for colliders as the decay products of the light scalars are difficult to reconstruct. In [49] my collaborators James Wells, Ben Sheff, and I identify new experimental observables which can help identify this Higgs to light scalars to photons decay chain and quantify the experimental inefficiencies which result from ignoring these observables.

1.6.2 Chapter 3: Axion-Like Particles at the ILC Giga-Z

Axion-Like Particles (ALPs) are a generic extension to the SM which appear in many models of spontaneous symmetry breaking. In [50], James Wells and I compute limits on ALPs which couple to hypercharge by examining the sensitivity of the ILC to Z decays involving an ALP and a photon.

1.6.3 Chapter 4: Discovering Axion-Like Particles with Photon Fusion at the ILC

Continuing examining the discovery capabilities of the ILC to ALPs, in [51] I examine the photo-production of ALPs in the Equivalent Photon Approximation (EPA) and their subsequent decay into pairs of photons. This unique channel allows for the production of ALPs with very large masses at the $250\,\mathrm{GeV}$ and $500\,\mathrm{GeV}$ stages of the ILC at weak coupling.

Chapter 2

Higgs Boson Decays Into Narrow Di-Photon Jets and Their Search Strategies at the Large Hadron Collider

Abstract: In many extensions of the Standard Model the Higgs boson can decay into two light scalars each of which then subsequently decay into two photons. The underlying event is $h \to 4\gamma$, but the kinematics from boosted light scalar decays combined with realistic detector resolutions may fail to register the events in straightforward categories and thus may be lost. In this article we investigate the phase space for highly boosted di-photon events from these exotic Higgs decays and discuss search strategies that aim to capture and label events in this difficult region. In the process we develop a new category, ξ-jets, which identifies with high selectivity highly collimated di-photon decay modes of the Higgs boson.

2.1 Introduction

Nearly a decade after the discovery of the Higgs boson it remains to be decided whether the discovered particle interacts with other known elementary particles in precisely the way the Standard Model dictates [52–57]. Deviations from SM expectations can arise by virtue of the Higgs boson being composite, part of a larger Higgs sector, coupled through its portal interactions to hidden sector states, or embedded in extra dimensions to name just a few examples. Alternatives remain viable because the SM Higgs boson couplings to other SM states are known only to at best 10% for some, and only to within $\mathcal{O}(1)$ factors for others, including muon, electrons, charm, and Higgs self interactions [58, 59]. The possibility of the Higgs boson decaying into final states that are not allowed by the SM is also not constrained well in many cases.

In this article we take up the case of the Higgs boson (h) decaying into other very light scalars

(ϕ_1 and ϕ_2) where each subsequently decays into photons,

$$h \to \phi_1\phi_2 \to (\gamma\gamma)(\gamma\gamma) \quad \text{(target observable)}. \tag{2.1.1}$$

In several different limits this process has been studied already [60, 61]. In the case of $\phi_{1,2}$ both having mass above about $10\,\mathrm{GeV}$ one finds that the events register as unambiguous 4γ events in the detector that can be searched for well. Within this regime, current studies limit this process to $B(h \to 4\gamma) \lesssim 3 \times 10^{-4}$ [62, 63].

On the other extreme, if $\phi_{1,2}$ both have mass less than a few hundred MeV, the photons from $\phi_i \to \gamma\gamma$ are so collimated coming from the highly boosted ϕ_i resultant from their parent Higgs decay, that each ϕ_i decay appears to go to a single photon. In that case, $h \to \phi_1\phi_2$ is simply combined with the standard $h \to \gamma\gamma$ analysis, and it becomes a statistical question to determine what overabundance of such a signal would be consistent with data. At 95% CL the answer to this question is that the branching fraction of non-SM contributions to $B(h \to \gamma\gamma)$ cannot exceed 2.2×10^{-4} [34]. Such light scalars may also be disentangled from the SM $h \to \gamma\gamma$ process with sophisticated substructure techniques [64, 65].

Combining both extremes leads to an apparent detection $h \to 3\gamma$. This arises when one of the ϕ_i has mass less than a few hundred MeV and the other more than about $10\,\mathrm{GeV}$. This process is forbidden in the SM, and the branching ratio is currently limited to $B(h \to 3\gamma) \lesssim \times 10^{-3}$, as can be gleaned from [66].

In between these two extremes, from the point of view of observables, is a murky region where the mass of one or both ϕ_i states is between $\sim 0.1\,\mathrm{GeV}$ and $10\,\mathrm{GeV}$. In that case, the two photons coming out of the ϕ_i decays are not highly collimated nor are they cleanly separated. Roughly speaking, the ATLAS and CMS detectors see something distinct from a standard photon but that also does not register as two photons when the photon separation is between $0.04 < \Delta R < 0.4$ [67, 68]. It is this difficult middle ground region that we wish to address in this letter.

It should be stated that extending the scalar sector of the SM by one (or multiple) singlets is a mature and well studied subfield [69–71]. Much of the parameter space for exotic heavy and light scalars (relative to the Higgs boson mass) is well constrained by direct searches and by precision electroweak measurements [44]. Our simplified model highlights a region of parameter space in a class of singlet extended models that has been less explored by previous studies.

The value in exploring such a regime lies in its ability to utilize the available experimental power from the LHC to investigate one of the most interesting loose ends in the Standard Model. Many models exist coupling new light scalars to the Standard Model in ways that are highly susceptible to the search strategy we advocate here [72]. The nature of the Higgs boson makes such couplings to new physics generic and apparent in a broad swath of theory parameter space. Furthermore,

the rough knowledge we have of the Higgs boson to date deserves significant tightening in every reasonable direction. Our goal here is to consider this particular case in detail, highlight the experimental challenges for discovery, proffer some suggestions, and suggest a benchmark theory with points that may be useful for serious further study by experimental groups within the ATLAS and CMS collaborations.

2.2 Theory description

The phenomenon we are after is $h \to \phi_1\phi_2$ with subsequent decay of $\phi_i \to \gamma\gamma$. Such decays arise generically in a broad class of BSM theories, many of which give rise to additional exotic phenomena. Most commonly these are other, similar gauge interactions, such as $Z \to \phi\gamma$, but the possibilities are wide and varied. Many BSM theories of this type are not yet constrained by experiment and have their most accessible phenomenon as $h \to \phi_1\phi_2 \to 4\gamma$, if there are dedicated searches for it. Our focus lies in this last type of theory.

To devise an experimental strategy and analysis to discover this class of targeted theories, we must begin by constructing a representative theory within the class and finding ways to find evidence for it. Ideally the representative theory should be maximally simple without losing the key features under consideration for our exotic Higgs decays. In this case, there is such a simple theory, and its lagrangian is

$$\begin{aligned}\mathcal{L} = \mathcal{L}_{\rm SM} &+ \frac{1}{2}(\partial_\mu\phi_1)(\partial^\mu\phi_1) + \frac{1}{2}(\partial_\mu\phi_2)(\partial^\mu\phi_2) - \frac{1}{2}m_1^2\phi_1^2 - \frac{1}{2}m_2^2\phi_2^2 \\ &+\lambda_\phi|H|^2\phi_1\phi_2 + \frac{1}{\Lambda_1}\phi_1 F_{\mu\nu}F^{\mu\nu} + \frac{1}{\Lambda_2}\phi_2 F_{\mu\nu}F^{\mu\nu} \ \ (\text{representative theory}) \qquad (2.2.1)\end{aligned}$$

where $F^{\mu\nu}$ is the photon field strength tensor. Of course, one could write down non-trivial $|H|^2\phi_1^2$ and $|H|^2\phi_2^2$ terms among others, but that would add complexity without contributing significantly to the final phenomenology. One might also object that $\phi_i F_{\mu\nu}F^{\mu\nu}$ should be traded in for gauge-invariant couplings of ϕ_i to hypercharge field strength tensor $\phi_i B_{\mu\nu}B^{\mu\nu}$ and $SU(2)$ field strength tensor $\phi_i W^a_{\mu\nu}W^{a,\mu\nu}$. That would be fine, except that upon diagonalizing these interactions to those of the mass eigenstates one finds nevertheless $\phi_i F^2$ terms, which will completely dominate in the decays of ϕ_i over $\phi_i Z^{\mu\nu}F_{\mu\nu}$ and $\phi_i Z^2$ terms due to the Z boson being much heavier than the ϕ_i that we will consider below.[1] The $\phi_i ZF$ interaction can give rise to $Z \to \phi_i\gamma$ decays, constrained by searches at the Tevatron and the LHC [62, 73], but as the scale of Λ_i becomes higher, this constraint goes away while $B(\phi_i \to \gamma\gamma)$ remains 100%[2]. For that reason we drop

[1] Barring any tuned cancellations, typical branching ratios to $\gamma\gamma$ are $10^7(10^{15})$ times larger than the branching ratios to $\gamma Z^*(Z^*Z^*)$.

[2] As the Λ_i increase, so does the decay length of the scalar. We have checked that the scalar decay length can be under $1\,\mathrm{mm}$ even for large (PeV) values of Λ_i which evade the $Z \to \phi_i\gamma$ constraint.

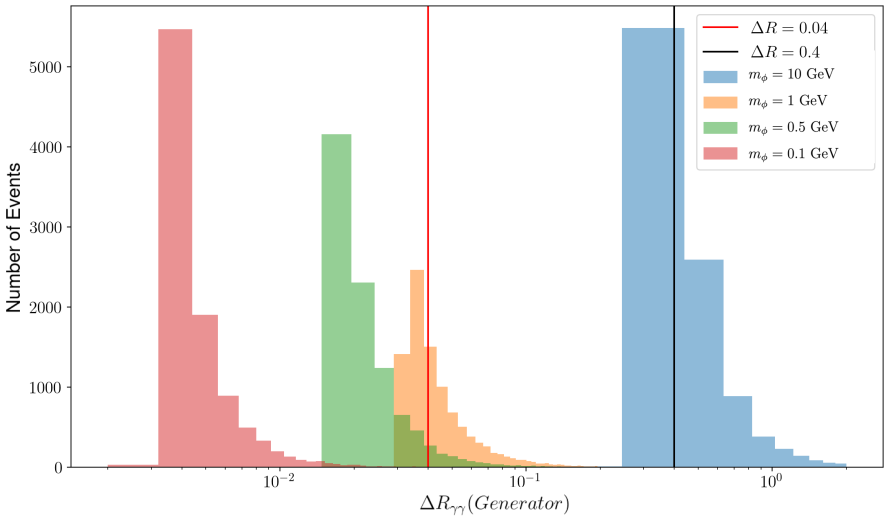

Figure 2.1: ΔR separation between photon pairs from ϕ_i decays, sampled over 10,000 events at varying masses of the BSM scalars.

these extra consideration and extraneous interactions from the theory description and retain only the lagrangian of Eq. 2.2.1.

From the point of view of devising experimental search strategies to find evidence for the Higgs boson decaying into a single light scalar, say σ such that $h \to \sigma\sigma \to 4\gamma$, the benchmark theory above is adequate. It merely corresponds to the case of $m_1 = m_2$. That is not to say the two theories are exactly the same, only that the subsequent search strategies are the same. That is why we propose to work with only one theory – the representative theory of Eq. 2.2.1 – which we believe to form a basis upon which benchmark points can be established and strategies devised.

2.3 Photon ξ-jets

As we mentioned in the introduction, the target observable of Eq. 2.1.1 implies photon separation from ϕ_i decays that is sensitive to the ϕ_i masses. This separation is given by

$$\Delta R_{\gamma\gamma} \sim 2m_{\phi_i}/E_{\phi_i} \sim 4m_{\phi_i}/m_h. \tag{2.3.1}$$

This is illustrated in Fig. 2.1, which shows that $m_\phi = 10\,\text{GeV}$ gives well separated photons ($\Delta R > 0.4$) and $m_\phi = 0.1\,\text{GeV}$ gives very collimated photons ($\Delta R < 0.04$), and mass of $1\,\text{GeV}$ gives intermediate separation. Recall that $\Delta R = \sqrt{(\Delta\phi)^2 + (\Delta\eta)^2}$, and $\Delta\phi$ is the azimuthal angle separation and $\Delta\eta$ is the pseudo-rapidity separation of the two photons in $\phi_i \to \gamma\gamma$ decay.

We turn to the ambiguous case in which the ϕ_i masses fall within the "intermediate mass" range of $1\,\mathrm{GeV} < m_{\phi_i} < 10\,\mathrm{GeV}$. Within the LHC environment, the production of Higgs bosons and their subsequent decay into such scalars yields photon pairs separated by

$$0.04 < \Delta R_{\gamma\gamma} < 0.4 \quad (\text{intermediate separation}). \tag{2.3.2}$$

It is well known that photon pairs that fall within the intermediate separation range of Eq. 2.3.2 are extremely difficult to separate or identity. We will speak much more on that below, but here we wish to pay respect to that difficulty by giving it a name. We call two photons that are within the range specified by Eq. 2.3.2 a "ξ-jet". The ξ-jet is a purely theoretical object, and it is defined by underlying "truth data" and not with respect to any detector performance. If a photon has another photon within the intermediate separation annulus of Eq. 2.3.2, and nothing else is within the outer ring of that annulus, then it ceases to be a photon and the two together form a ξ-jet. Such a concept can be generalized to more than two photons but it is of not much importance here to do that. We also specify as a theoretical object that a photon is defined to be either a single photon or two photons within $\Delta R < 0.04$ of each other.

With these theory definitions of photon and ξ-jet, our target observable is broken into several distinct and non-overlapping final states, depending on the masses of the ϕ_i intermediate states in the decay chain:

$$h \to \phi_1\phi_2 \to 4\gamma \;\Rrightarrow\; 4\gamma,\; 2\gamma,\; 3\gamma,\; \gamma\xi,\; \gamma\gamma\xi,\; 2\xi \quad (\text{observable partitions}) \tag{2.3.3}$$

The first three of these observables we have already discussed. The remaining observables have not been fully explored in the literature, and we wish to consider them in more detail below.

2.4 Benchmark model points

We are interested in exploring three observables: $\gamma\xi$, $\gamma\gamma\xi$, and 2ξ. To do so we need benchmark points that give rise to each of these types of observables. They can be obtained rather straightforwardly from our representative theory of Eq. 2.2.1 where the masses of ϕ_1 and ϕ_2 are chosen to be various permutations of the masses $0.1\,\mathrm{GeV}$, $1\,\mathrm{GeV}$ and $10\,\mathrm{GeV}$. In particular, $m_\phi = 0.1\,\mathrm{GeV}$ generally always gives $\phi \to \gamma$ decays, $m_\phi = 1\,\mathrm{GeV}$ typically gives $\phi \to \xi$ decays, and $m_\phi = 10\,\mathrm{GeV}$ generally gives $\phi \to \gamma\gamma$ decays according to our definitions in the previous section. These are so far entirely defined theoretically. In the next section we will pursue more carefully how a theoretical ξ-jet registers in an experimental analysis.

From these considerations we can construct the following four benchmark points A, B, C, and D specified in Table 2.1. Fig. 2.2 shows the relative fraction of each observable for each benchmark

Point	m_1 (GeV)	m_2 (GeV)	Dominant mode	Subdominant mode
A	1	10	$\gamma\gamma\xi$	$\gamma\xi \simeq 2\gamma \simeq 3\gamma$
B	0.1	1	$\gamma\xi$	2γ
C	1	1	2ξ	$\gamma\xi \simeq 2\gamma$
D	0.1	10	3γ	$\gamma\xi$

Table 2.1: Benchmark points for $h \to \phi_1\phi_2 \to 4\gamma$ which then partition into various theory-object observables (modes) according to our definitions of ξ (photon pairs with $0.04 < \Delta R < 0.4$) and γ (an isolated photon with $\Delta R > 0.4$ or two photons within $\Delta R < 0.04$).

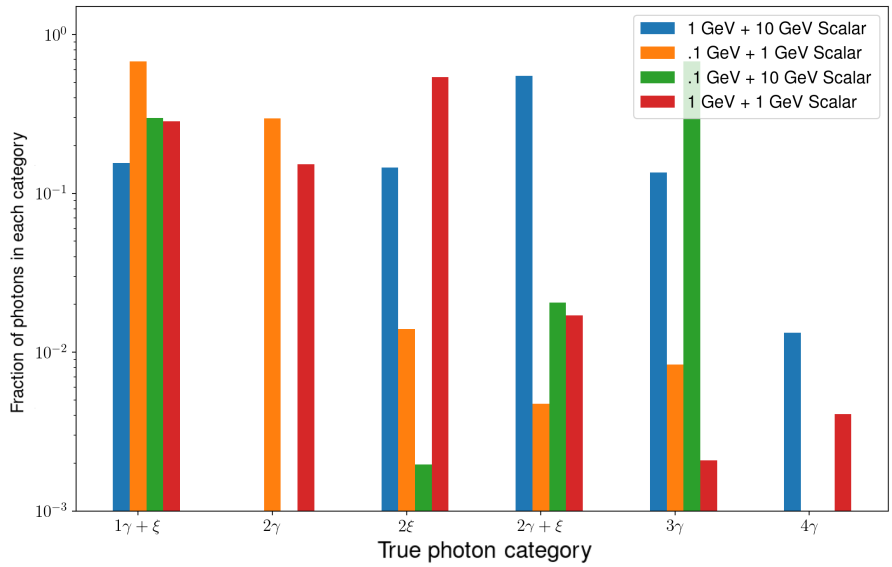

Figure 2.2: Branching fraction into each final state theory observable for the benchmark points A (blue), B (orange), C (red) and D (green) given in Table 2.1.

point. The dominant and subdominant modes of decay for each benchmark point are listed in Table 2.1 and can be gleaned from the fraction data given in Fig. 2.2. Table 2.1 shows that several combinations of light scalar masses give interesting decay signatures involving combinations of ξ-jets and photons which (to the authors' best knowledge) are not being searched for in current LHC analyses.

2.5 Experimental search strategies

So far our discussion has been mainly theoretical. We have identified a rare Higgs decay whose cascade we claim may be difficult to detect by experiment. In this section, we discuss how our theoretical objects translate into experimental manifestations. We have suggested that some

mass ranges of ϕ_i are problematic for experiment. We will discuss some details on why they are challenging and some strategies by which to possibly overcome those challenges.

2.5.1 Multi-photon final states

Isolated photons or extremely highly collimated photons both get identified simply as photons, and analysis based on those standard objects (photons) proceed without much subtlety regarding how to process the data into well-defined final states of 2γ, 3γ and 4γ.

2.5.2 ξ-jet final states

Some of the final states from the decays of Eq. 2.3.3 yield ξ-jets. Underneath, a ξ-jet is merely two photons with intermediate ΔR separation (see Eq. 2.3.2). But a key question is, how does a ξ-jet, defined as a theoretical object, get processed into various experimental categories? A perfect detector would register it as merely two photons, a bad detector as a single photon or nothing, and a realistic good detector, such as ATLAS or CMS, registers it as something altogether different within several possible categories of varying sensitivity and selectivity[3].

To address this question of how a ξ registers in a detector it is useful to describe the various categories into which a single photon can fall. As an example we take the standard categories which ATLAS uses for photon identification. There are eight possible standard categories, six are the permutations among three isolation possibilities (non-isolated, loose isolation, and tight isolation) and two ID possibilities (loose ID and tight ID). The other two categories are jet and "lost." Jet is the standard QCD jet from fragmentation of quarks or gluons, and "lost" refers to the possibility that the data does not conform to any other category and is not registered in any higher abstracted category except for mere energy depositions in the detector.

A ξ-jet will register with some probability into one or more of the standard photon categories. The probability to do so depends on the underlying event kinematics. Under typical assumptions, the ξ-jet will often register as "lost" due to the inability to resolve the two photons yet the event covers more than one cell in the electromagnetic calorimeter which a single photon would not do. As no category becomes applicable, it has no option but to be relegated to "lost."

The implication of a ξ-jet arising from a Higgs decay being categorized as "lost" is that an analysis that requires reconstructing the invariant mass of the Higgs boson from well-defined decay products can no longer register the events. It is therefore necessary to build a ninth category "ξ-

[3]By perfect (non-existent) "sensitivity" we mean a category test that passes with 100% (0%) rate if the underlying event is a ξ-jet, and by perfect (non-existent) "selectivity" we mean a category test that passes with 0% (100%) rate if the underlying event is not a ξ-jet. Good sensitivity means low false negative rate, and good selectivity means low false positive rate.

candidate" under which ξ events can fall. ξ-candidates must be defined entirely through detector response, with the goal of producing high sensitivity to underlying ξ-jets with reasonably good selectivity (i.e., mostly only ξ-jets register as ξ-candidates).

2.5.3 ξ-candidates

A detailed definition of the "ξ-candidates" category satisfying the demands stated above is best constructed by a team of experimental experts within the ATLAS and CMS collaborations deeply familiar with their detectors. However, it is likely that such a definition meeting the demands of sensitivity and selectivity will have several key characteristics which we would like to discuss here. We will then make illustrative estimates of the utility of a ξ-candidates definitions based on these characteristics.

We make use of MadGraph_aMC@NLO [74] simulations to produce our signal events at leading order with the lagrangian of Eq. 2.2.1, which are then hadronized via PYTHIA8 [75, 76]. For our detector studies we utilize Delphes [77] fast detector simulation framework with the default CMS card and FastJet [78] for jet clustering algorithms.

To begin one must have a cluster, established by standard techniques. One useful criteria to impose on the pre-ξ-candidate cluster is a strong isolation requirement against QCD activity within a small cone around the ξ-candidate system, reducing QCD backgrounds from decaying pions. Additional criteria for the definition must also appeal to the stoutness of the photon jet — there are two photons separated enough to not look like one photon and that separation shows up as a larger-than-normal spatial spread among cells within the electromagnetic detector. Furthermore, vetoing on charged tracks eliminates electron-induced showers. Finally, recently established jet n-subjettiness algorithms [79] can be employed to select clusters that have discernible sub-jet structure compatible with 2 collimated photons. Refs. [64, 80] go into detail on the ability to use these and other, similar variables to separate ξ-candidates (called photon-jets in these papers) from photons and QCD jets, but all of these considerations will be in play in the definitions below.

Our ξ-jet theory definition was for underlying two-photon clusters with ΔR separation in the range of 0.04 to 0.4. In addition, within the range of $0.025 < \Delta R < 0.04$ there is a possibility of using electromagnetic shape variables to discern that the underlying event was likely not a single photon, but certainly not clear enough to indicate the possibility of two photons. Nevertheless, our ξ-candidate list of criteria will be applicable for two-photon jets separations down to about $\Delta R \gtrsim 0.025$ and up to about $\Delta R \lesssim 0.25$. We will not discuss the range $0.25 \lesssim \Delta R \lesssim 0.4$ here, because our understanding is that more traditional photon identification tools may be applicable to separate the photons just well enough to help discern signal from photon backgrounds.

Let us now turn to a more precise definition of ξ-candidates (underlying two-photon separation

Variable	Definition	Cut	Reasoning
$\log\theta_J$	hadronic energy fraction	< -0.8	exclude QCD and τ
N_T	Number of tracks	= 0	excludes single converted photons and jet activity
τ_2/τ_1	Ratio of 2- to 1-subjettiness	< 0.3	Selects events with 2 subjets

Table 2.2: ξ definition meant to capture underlying events with $0.025 < \Delta R < 0.25$. These objects are defined as a cone of radius $\Delta R = 0.25$ about a central cluster in the EM calorimeter, centered on the highest energy pixel. Unless otherwise stated, the region is within the ξ region. Here θ_J is the hadronic energy fraction.

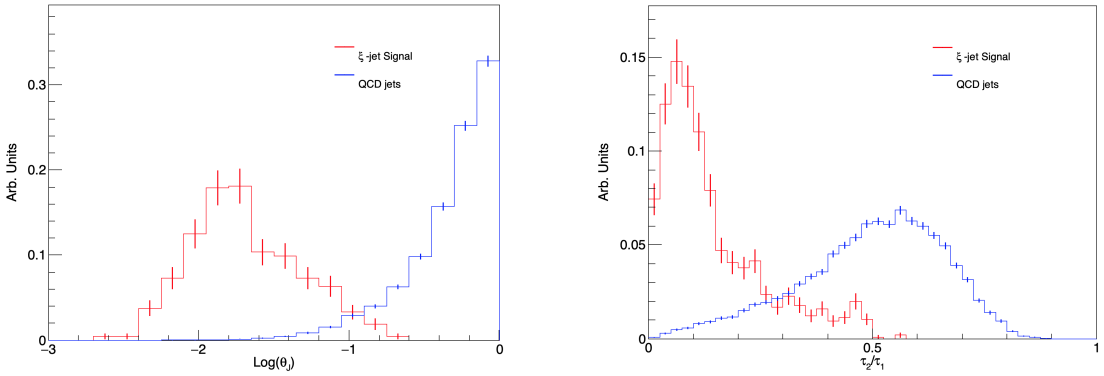

(a) (b)

Figure 2.3: Subset of kinematic variables useful for discriminating of ξ-jets (green) and QCD jets (blue) which are a major background. Here θ_J is the hadronic energy fraction for a jet, and τ_2/τ_1 is the ratio of 2-jettiness to 1-jettiness which is useful for picking out events with 2 subjets.

$0.025 \lesssim \Delta R \lesssim 0.25$). This regime targets events that have two photons in sufficiently close proximity that their cores overlap, thereby interfering with one anothers' identification procedure. This should appear as a cluster of energy in the EM calorimeter, with no tracks or corresponding energy in the hadronic calorimeter, and high 2-subjettiness. We provide an example definition of ξ-candidate criteria in Table 2.2. Below in Fig. 2.3 we also show distributions of signal and background for QCD jets and ξ-jets. These distributions reproduce those of [64, 80] and show that ξ-jets can be separated from QCD backgrounds with high efficiency.

2.5.4 Reconstructing ξ-jets and Higgs decays

Now that we have precise definitions of photons and ξ-candidates we can ask how well the Higgs boson signal can be reconstructed, especially in the case of its decay into one or more ξ-jets. Fig. 2.4 shows the analysis flow of our reconstruction of ξ-jets using Delphes fast detector simulation. Additional photons not covered by that flow, as well as electrons, muons, jets, etc. are

identified and labeled by other analysis flows.

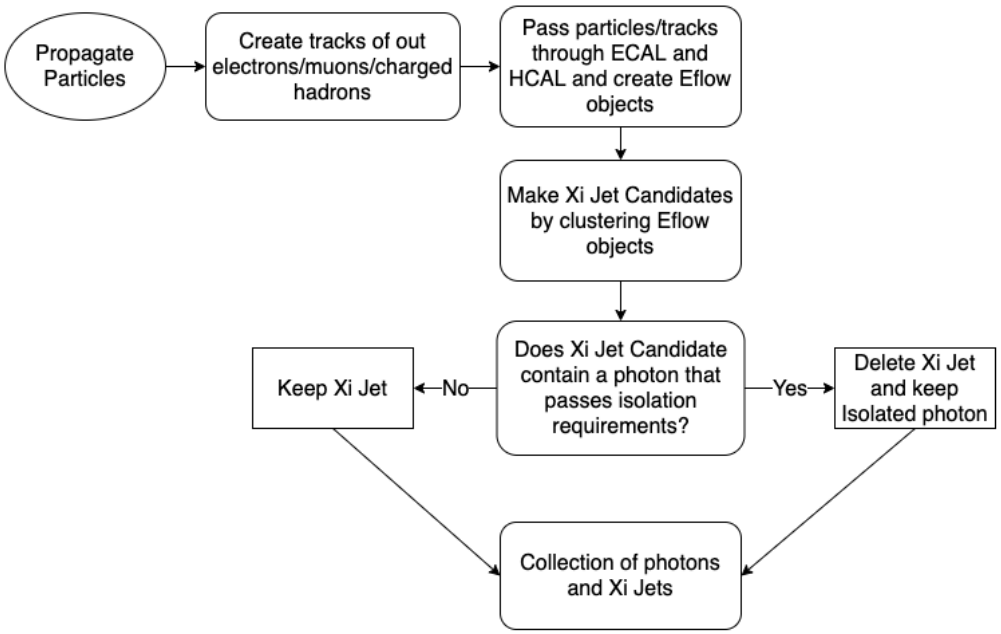

Figure 2.4: the analysis flow of our reconstruction of ξ-jets using Delphes fast detector simulation. Additional photons not covered by that flow, as well as electrons, muons, jets, etc. are identified and labeled by other analysis flows.

First, one must reconstruct the ξ-jets which we attempt to do by following a strategy similar to Ref. [64]. The method is as follows. First energy flow (eflow) objects [81] (composed of deposits in calorimeter cells) are clustered into jets using the anti-kt algorithm with $R = 0.25$. Then we re-cluster those energy deposits that were found in each jet using the kt algorithm, which determines a recombination tree for the jets. This tree specifies the subjets at each level of recombination N from $N = 1$ (the full jet) to $N =$ the number of constituent eflow objects in the jet (no recombination). From here we can compute the N-subjettiness variable for the jet for each N. This variable becomes small when the parameter N is large enough to describe all of the relevant substructure of the jet. It is defined to be

$$\tau_N = \frac{\Sigma_k p_{T_k} \times \min[\Delta R_{1,k}, \Delta R_{2,k}, ..., \Delta R_{N,k}]}{\Sigma_k p_{T_k} \times R}, \tag{2.5.1}$$

where k runs over all the constituents of the jet, p_{T_k} is the transverse momentum for the k-th constituent, and R is the characteristic jet radius used in the original jet clustering algorithm.

After jet clustering is completed we then check if a reconstructed ξ-candidate already contains a reconstructed photon. Reconstructed photons are composed of eflow objects originating from the ECAL which must pass isolation requirements (cuts on electromagnetic and hadronic activity

within a cone around the photon). If a ξ-candidate contains an already reconstructed, isolated photon then this ξ-candidate is deleted.

Before applying additional cuts, we would like to characterize the efficiency at which we reconstruct ξ-jets. To do this we utilize Delphes GenJet objects. GenJets are jets that are clustered, not with calorimeter cells or towers or eflow objects, but with the actual generator level particles. By utilizing GenJets we can define "generated ξ-jets" and see at what rate we correctly reconstruct these.

GenJets are clustered with the same strategy as above, first with the anti-kt algorithm with $R = 0.25$, and then reclustered with the kt algorithm. A GenJet is selected as a generated ξ-jet if it has: 1) At most two photons with $p_T > 0.5$ GeV, 2) no non-photons with $p_T > 0.5$ GeV. Since our theoretical ξ-jets were defined as pairs of photons with ΔR between 0.04 and 0.4, we throw out ξ-jets with $\Delta R < 0.025$ as these will most likely be reconstructed as one photon.

Once a generated ξ-jet is identified, we loop over all reconstructed ξ-candidates and attempt to find a match. Matching is done by comparing the ΔR between the momentum of the generated and reconstructed jets. If $\Delta R_{gen/reco} < 0.05$ we consider this jet as matched. We also require that the reconstructed ξ-jets pass a cut on the required hadronic energy fraction. This cut is that $\log(E_{had}/E_{jet}) < -0.8$. Below in Fig. 2.5 we show $\Delta R_{gen/reco}$, which shows the level of matching between generated and reconstructed ξ-jets. It also serves as a check that this is independent of our model parameters.

Now we would like to understand how often we can reconstruct the Higgs mass using our reconstructed photons and ξ-candidates. To simplify matters we will choose $m_{\phi_1} = m_{\phi_2}$, which is equivalent to having only one light scalar in addition to the observed h_{125}. We scan over light scalar masses from 100 MeV to 14 GeV. This range ensures we see a smooth transition between photon dominated decays and ξ-jet dominated decays. The following discussion can be generalized by choosing different masses for the light scalars. After reconstruction, we first collect all of our reconstructed objects, which for now are photons and ξ-candidates. We only require our reconstructed ξ-candidates to pass our hadronic energy fraction cut, otherwise no cuts (besides minimum p_T cuts which are used for clustering). We then form all the possible subsets of this collection, which have between 1 and 4 objects (as at most the Higgs decayed into 4 separable photons). If one combination of ξ-candidates and photons yields an invariant mass within a 3 GeV window around 125 GeV (122 GeV $< M_{inv} <$ 128 GeV) then we consider this a match. Virtually no events contain multiple combinations of photons and ξ-jets which satisfy this requirement. We split each match into the following categories based on what number and type of objects make up the matching set.

1. Photons only: Matches with 2, 3, or 4 photons

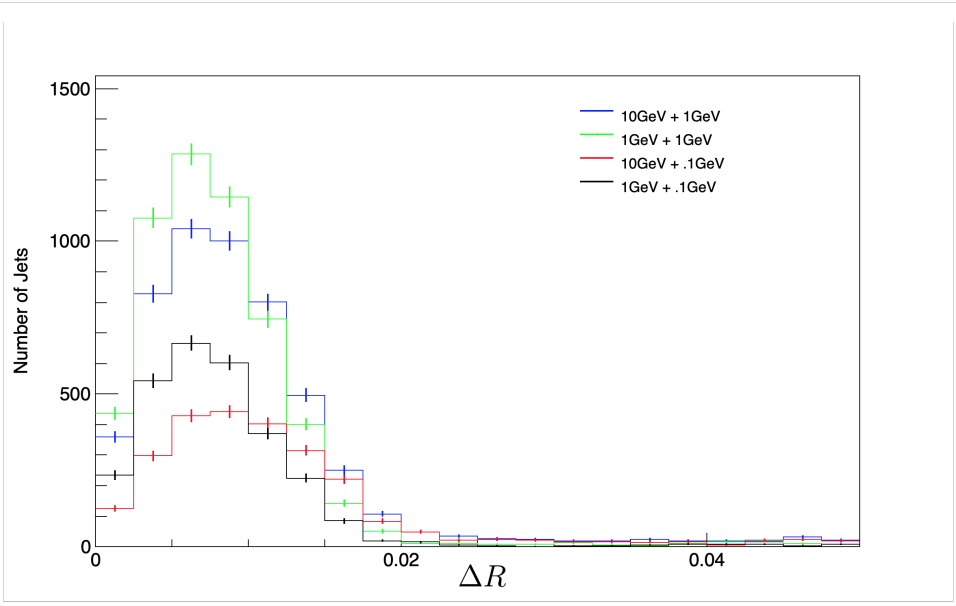

Figure 2.5: ΔR between reconstructed and generated ξ-jets. Distribution is independent of our model parameters showing good matching between the two.

2. Photons + ξ-jets: Matches with 1 photon + 1 ξ, 2 photons + 1 ξ
3. ξ-jets only: Events with 2 and only 2 ξ-jets
4. ξ-jets inclusive: Includes the Photons + ξ-jets category as well as the ξ-jets only category
5. Other combinations: Any combination not included above
6. All: Any match in the accepted mass range

Fig. 2.6 then shows the efficiency of reconstructing the Higgs mass as a function of the light scalar mass. Several key observations can be made here. At very low scalar masses, photons only makes up the dominant signal channel as the pairs of photons from ϕ decay are extremely collimated. From 100-300 MeV the signal from photons + ξ jets becomes the most efficient channel as one of the pairs of photons is collimated enough to form a ξ-jet. Immediately above 300 MeV the signal from pairs of ξ-jets (ξ-jets only) becomes an order of magnitude more efficient than the photon only channel and remains so until 6 GeV. Overall, searches including ξ-jets are more than an order of magnitude more efficient at reconstructing the Higgs from masses between 100 MeV and 10 GeV.

Fig. 2.6 shows that searches including ξ-jets would be invaluable if a light scalar connected to the gauge and Higgs sector as in Eq. 2.2.1 exists in nature. We would like to stress that even

though our analysis and definitions are quite simple, our results should be robust even after the introduction of more strict experimental search strategies and analysis cuts. It is interesting to compute how many such ξ-jet events one could expect for a given luminosity at the LHC. This is of course a function of the ϕ mass and the efficiency for reconstructing the h_{125}. To give an estimate, we can take the $m_\phi = 2$ GeV point as an example. This has an efficiency for reconstruction of about 50%. If we take Br($h \to \phi\phi$) = 10^{-4} and an integrated luminosity of 300 fb^{-1}, this leaves us with about 7500 reconstructed events.

While a comprehensive study of standard model backgrounds is necessary for an experimental search, we can still make qualitative statements about discriminating ξ-jets from objects which fake ξ-jets. The largest backgrounds will be from jj, and $\gamma\, j$ production where a QCD jet fakes a ξ-jet. References [64, 80] use a Boosted Decision Trees based on energy and substructure variables to discriminate between QCD jets and photon jets. They quote a fake rate from QCD jets of $10^{-4} - 10^{-5}$, though this fake rate is dependent on the rate at which one accidentally rejects ξ-jets. Additionally, the requirement that the invariant mass of the two ξ-candidates needs to fall within a 3 GeV window of the h_{125} mass lowers the background as well, as the rate for QCD jet production tends to fall at high invariant masses. Combined, these factors should allow for a bump hunt search for ξ-jets with high sensitivity.

Lastly we would like to comment on our results in comparison to other results in the literature concerning similar rare Higgs decays to scalars. It is our understanding that these articles are principally concerned with only the separation of photon jets and non photon jets, e.g. analyzing purity and efficiency for photon jets vs. single photons and other QCD related jets. In contrast, we have tried to paint a picture which quantifies how such rare Higgs decays to ϕ_i can be missed if only traditional techniques involving photons are used. In providing a clear theoretical and experimental definition of a photon and a ξ-jet we have been able to provide concrete branching fractions to states involving combinations of ξ-jets and photons only in terms of observables, that which a detector actually measures. The extremely high ratio of events involving ξ-jets to events involving only photons serves as a testament to the need for such an analysis. We hope that this can guide future experimental inquiries into models such as 2.2.1.

2.6 Conclusion

The discovery of the Higgs boson has lent strong support to the Standard Model, but also has allowed us to search for new avenues along which to extend it. In this work we have investigated exotic decays of the 125 GeV Higgs boson into light scalars which as of yet may be missed via current analysis techniques. We have discussed, first theoretically and then experimentally, a new object dubbed a ξ-jet which could play a pivotal role in the discovery of any light scalars

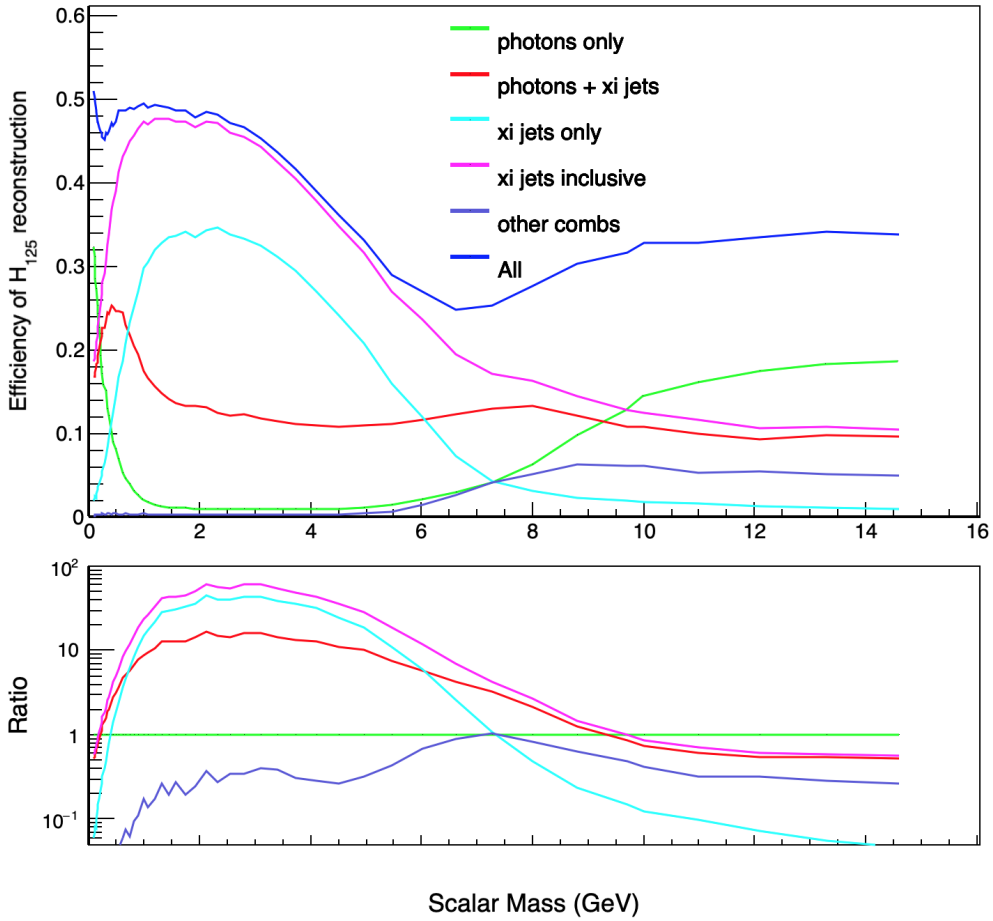

Figure 2.6: Top: Efficiency of h_{125} reconstruction as a function of scalar mass split into different categories based on number of ξ-jets and photons. Bottom: Ratio to only using photons. The reconstruction efficiency is more than an order of magnitude better when including ξ-jets (pink) over a wide range of masses from 100 MeV to 10 GeV. More specifically, the 2 ξ-jet channel dominates from the range of 300 MeV to 6 GeV.

minimally coupled to the standard model Higgs and to photons as in Eq. 2.2.1. If experimentalists are able to identify and reconstruct ξ-jets these new objects could be strong evidence for an extended Higgs sector and Beyond the Standard Model physics.

Chapter 3

Axion-Like Particles at the ILC Giga-Z

Abstract: Axion-Like Particles (ALPs) are a generic, calculable, and well motivated extension of the Standard Model with far reaching phenomenology. ALPs that couple only to hypercharge represent one subset of such models, coupling the ALP to both photons and the Z boson. We examine the current constraints on this class of models with an ALP mass in the 100 MeV to 100 GeV range, paying particular attention to the region between 100 MeV to 10 GeV, a portion of parameter space which is ill constrained by current experiments. We show that the more than 10^9 Z bosons produced in the Giga-Z mode of the future ILC experiment, combined with the highly granular nature of its detectors, will allow for ALPs coupled to hypercharge to be discovered with couplings down to nearly $10^{-5}\,\mathrm{GeV}^{-1}$ over a range of masses from 0.4 to 50 GeV.

3.1 Introduction

One of the simplest BSM scenarios comes from augmenting the Standard Model with new singlet (pseudo)scalar particles. Such models have rich phenomenology despite their simplicity, and can influence the structure of the Electroweak phase transition [82], provide natural dark matter candidates [83, 84], and can be naturally accommodated in well motivated UV models [85]. One class of new light scalars is the Axion-Like Particle (ALP) [86, 87]. An ALP is defined as a relatively light pseudo-scalar that couples to two gauge bosons and possibly SM fermions. These particles are particularly well motivated as solutions to the Dark Matter and Strong CP problems [29] via the PQ mechanism, but can appear generically as pseudo Nambu-Goldstone bosons of spontaneously broken approximate symmetries or descend from phenomenogical string theory models. Regardless of their origin, ALPs are an extremely general extension of the SM and serve as a test case for investigating BSM physics. In addition, as the LHC and other experiments search for new physics in the form of heavy ($M \gg M_W$) particles, ALPs serve as an orthogonal but complementary search direction for theorists and experimentalists, as they are generally low mass but very weakly coupled. Fortunately, we will show that the next generation of lepton colliders like the ILC will provide clean signatures to weakly coupled ALP physics at the $\mathcal{O}(10^{-5}\,\mathrm{GeV})$ level for a range of interesting masses near and below the weak scale.

Many dedicated search strategies have been developed to study their production and influence on cosmology and particle physics, depending on the exact nature of the ALP in question [88]. In more detail, these searches depend on which gauge bosons the ALPs couple to, e.g. $U(1)_Y$, $SU(2)_L$, or $SU(3)_C$, and whether the the ALP couples to the SM fermions. In an effective field theory approach each of these couplings should be allowed, but each can be taken to be independent (modulo renormalization group (RG effects) [89,90]), allowing one to examine each portal one at a time. In this paper we take up one ALP model where our Axion-Like Particle, a, couples only to hypercharge through a dimension 5 interaction,

$$\mathcal{L} = \mathcal{L}_{\mathrm{SM}} + \frac{1}{2}\partial_\mu a \partial^\mu a - \frac{1}{2}m_a^2 a^2 - \frac{g_{aBB}}{4} a B_{\mu\nu}\tilde{B}^{\mu\nu} \ \ (\text{representative theory}). \tag{3.1.1}$$

Here, m_a is the tree level mass of the ALP which couples to hypercharge via the dimensionful coupling g_{aBB}, and $\tilde{B}^{\mu\nu} = 1/2\varepsilon^{\mu\nu\alpha\beta}B_{\alpha\beta}$ is the dual hypercharge field strength tensor. Of course many other effective Lagrangians involving couplings to additional gauge bosons and fermions would be equally valid to write down, but the resulting phenomenology is either qualitatively similar or produces orthogonal observables which would not affect subsequent discussion. Note, that several other authors study ALPs below the weak scale which couple purely to $F\tilde{F}$ rather than to $B\tilde{B}$. In the former case, the ALP couples only to photons and cannot couple to the Z. We choose to study the latter, $aB\tilde{B}$ operator, because in a gauge invariant, UV completion of

any model including an ALP there are likely to be $\mathcal{O}(1)$ connections between operators coupling the ALP to each of the electroweak gauge bosons. Thus we would like to put ALP-photon couplings on equal footing with ALP-Z/W couplings. This, as we shall see below, opens up further experimental discovery channels.

3.2 ALPs in Rare Z Decays

Much of the parameter space of this particular model, shown in Fig. 3.1, is highly constrained by terrestrial experiments [91], as well as cosmology and astrophysics [92, 93]. Light shining through wall (LSW) experiments and helioscopes constrain ALP masses up to several eV, and down to $g_{aBB} = 10^{-11}\,\mathrm{GeV}^{-1}$, while cosmology and astrophysical constraints cover larger masses in the eV to GeV range and couplings down to $10^{-12}\,\mathrm{GeV}^{-1}$ and lower. Complimentary

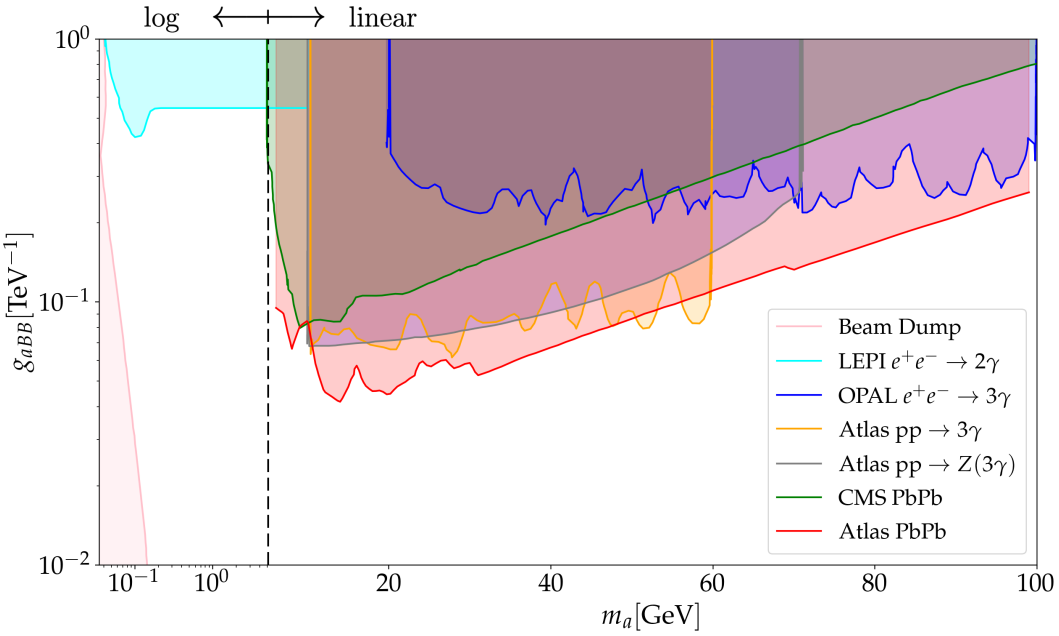

Figure 3.1: Current constraints on ALP model with hypercharge coupling. Figure adapted from [3–7].

constraints can be obtained with colliders and beam dump experiments, which can probe masses in the MeV to TeV range. ALPs produced at beam dumps penetrate shielding and then decay to pairs of photons which are detected by a downstream detector. These experiments rely on relatively smaller ALP couplings than colliders as the ALP has to travel a macroscopic distance to make it through the shielding and reach the downstream detector. Future experiments like the ForwArd Search ExpeRiment at the LHC(FASER) and DarkQuest will probe ALP-photon couplings around $10^{-3} - 10^{-6}\,\mathrm{GeV}^{-1}$ in 10 MeV - several 100 MeV range [94, 95]. Collider searches

target ALP production in association with a photon, with the ALP either leaving the detector leading to missing transverse energy (MET), or decaying in the detector volume leading to displaced vertices or other identifying signatures. Belle II (not shown in Fig. 3.1) for example searches for ALPs in $e^+e^- \to a\gamma \to 3\gamma$, and has found constraints of $g_{a\gamma\gamma} < 10^{-3}\,\mathrm{GeV}^{-1}$ in the mass range of 0.2 GeV to 10 GeV [96].

Interesting constraints also come from light by light scattering at the LHC in PbPb collisions. Here, the $\gamma\gamma$ scattering cross sections are enhanced by a factor of Z^4 [7], where Z is the number of protons in the nucleus. The presence of an ALP which couples to photons would enhance the light by light scattering ($\gamma\gamma \to \gamma\gamma$) cross section. Measurements of this cross section at CMS and ATLAS place constraints on Axion-Like Particles coupling to photons from 5 to 100 GeV down to a few $\times 10^{-4}$ GeV [4,5,7], competitive with LEP and other LHC searches over this mass range.

We would like to mention the analysis by Bauer et al. in [97] where the authors consider the ALP discovery prospects of the FCC-ee, HL-LHC, CLIC, and other future experiments in the context of a similar ALP model in the MeV to TeV mass range. Their analysis concludes that these experiments will probe ALP-photon couplings via associated ALP production, and rare Z and Higgs Decays down to $10^{-6}\,\mathrm{TeV}^{-1}$ for certain ranges of masses. We caution that a detector level analysis with realistic cuts and a thorough background analysis will most likely weaken the claimed sensitivities. Bauer et al. also examine precision EW constraints on massless ALPs, and find constraints at the $(1\,\mathrm{TeV})^{-1}$ level which is weaker than direct collider constraints. We expect the analogous constraints on massive ALPs to also be weaker.

After electroweak symmetry breaking the ALP develops a coupling to both the Z boson and to the photon, opening up the decay of an on-shell Z into an ALP and a photon with width

$$\Gamma_{Z\to a+\gamma} = g_{aBB}^2 s_W^2 c_W^2 \frac{(m_Z^2 - m_a^2)^3}{96\pi m_Z^3}. \tag{3.2.1}$$

As long as the ALP has a mass less than m_Z, it will then decay to two photons with a branching ratio of nearly 1. It can of course decay to other standard model particles at loop level but these will be heavily suppressed. This leads to the decay chain $Z \to 3\gamma$ or "tri-photon" signature.

Whether the ALP will promptly decay or lead to a displaced vertex depends on the ALP mass and hypercharge coupling, with the decay length given by $l = c\tau = \gamma_a/\Gamma_{a\to\gamma\gamma}$, where $\gamma_a = E_a/m_a$ is the boost factor of the ALP. While dedicated searches for displaced vertices and or MET lead to interesting constraints [98, 99], this note will focus on masses and couplings which lead only to prompt decays. This is shown in Fig. 3.2 for $m_a = 0.4, 1.0, 5.0, 10$ GeV. For $m_a \geq 0.4$ GeV and for couplings which can be probed by the ILC, all decays are prompt (decays occur prior to ALP entering the ECAL at the ILC).

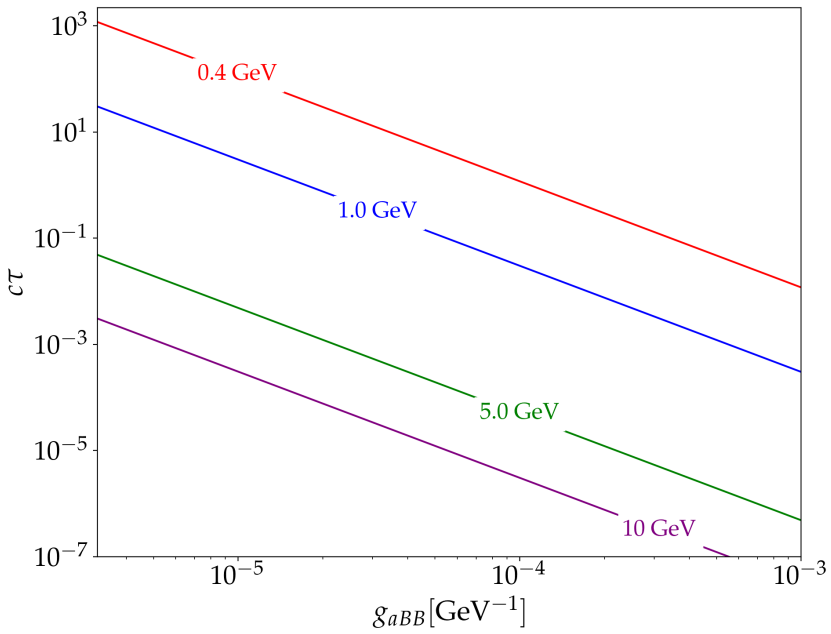

Figure 3.2: Proper decay length as a function of g_{aBB} for several different ALP masses.

$Z \to 3\gamma$ is an interesting final state to search for as it is absent at tree level in the SM, but loop induced with a tiny branching ratio of $\approx 10^{-9}$ [100]. This rare decay has been searched for by LEP, the Tevatron, and the LHC in an effective field theory context searching for SM induced and higher dimensional operator induced (anomalous) $Z\gamma$ couplings [6, 73, 101], with no excess over the SM background being found, establishing an upper limit of $B(Z \to 3\gamma) < 2.2 \times 10^{-6}$. Translating this into the (m_a, g_{aBB}) plane leads to the constraint $g_{aBB} < 10^{-4.5}\,\mathrm{GeV}^{-1}$, for masses large enough where the two photons from the ALP decay can be independently resolved. The exact value of the ALP mass, m_a, which leads to well separated decay photons depends on the details of the experimental analysis and detector and cannot straightforwardly be pinpointed, though it should lie at least above 10 GeV. Below $\mathcal{O}(10\,\mathrm{GeV})$ lies a subtle region of parameter space in collider searches which is the subject of this paper.

In dedicated ALP searches at experiments like the LHC and LEP, analyses are limited by their ability to reconstruct collimated pairs of photons [102]. Low mass ALPs produced from on-shell Z decays, subsequently decay into pairs of photons with a ΔR separation which peaks at $4m_a/m_Z$. Here $\Delta R = \sqrt{\Delta\phi^2 + \Delta\eta^2}$ is the angular distance measure between particles. ALPs with masses between 1 and 10 GeV tend to decay to collimated photon pairs which will overlap in a detector and thus not be correctly reconstructed as two individual photons. See [49] for a discussion on reconstructing overlapping photons at the LHC. At the LHC and in the LEP experiment, photons must be separated from charged particles and other photons by a $\Delta R >$

0.2, though this requirement depends on the details of each detector as well as the algorithms responsible for reconstructing photons. This should be taken as a rule of thumb. If a photon does not meet these requirements it is not reconstructed and rejected as a photon candidate. Above $m_a = 10$ GeV, the photons are well separated enough to be efficiently reconstructed. Low mass ALPs ($m_a < 1$ GeV) can be searched for in a two photon analysis as the two photons from the ALP decay tend to be collimated enough to register as one photon in a detector.

In [3] this was used to recast the LEP search for $Z \to 3\gamma$ in the $e^+e^- \to \gamma\gamma(\gamma)$ measurement into limits on the ALP model. In different ALP mass regions, $m_a < m_{\pi^0}$, $m_{\pi^0} < m_a < 10$ GeV, and $m_a > 10$ GeV, either searches for two or three photons were used based on whether the photons from the ALP decay would be well separated or not. This was used to set leading bounds on ALP masses and couplings between 100 MeV and 90 GeV, with the weakest bounds being in the intermediate mass regime of 1 GeV to 10 GeV. Though jet substructure techniques can be used to disentangle collimate pairs of photons from single photons [103], an experiment that can resolve individual photons via a granular detector in this ALP mass regime is crucial to enhance discovery prospects and increase our sensitivity to new physics with the same decay topology.

The International Linear Collider (ILC) represents exactly this opportunity to search for this rare decay in the sought after intermediate mass regime. Recent advances in photon identification algorithms, combined with the highly granular ILC detectors can allow for photon identification with much more relaxed photon separation requirements, meaning photons can be much closer to other charged particles and other photons. In the next section we will investigate to what extent the ILC can improve on past searches for $Z \to a\gamma \to 3\gamma$.

3.3 ILC and Photon Reconstruction

The ILC is a next generation, high luminosity, linear e^+e^- collider designed for high precision SM and BSM physics measurements [104–106]. The collider, though nominally designed to operate at 250 GeV center of mass energy, can be adjusted to run at a variety of center of mass energies, including operating at the Z pole. Operating the ILC at $\sqrt{s} = m_Z$ is dubbed the Giga-Z mode of the ILC, as the ILC will produce on the order of 10^9 or greater Z bosons, orders of magnitude more than the LEP physics program. This will result in drastic improvements in precision Z measurements, and measurements of $\sin^2\theta_{\text{eff}}$. Production of this many Z bosons will also allow for the search for rare decay modes, one of which is $Z \to 3\gamma$.

We first begin with a discussion of photon reconstruction at the ILC. Photon identification can be done via the GARLIC photon reconstruction algorithm [8] which was developed by the International Large Detector (ILD) group. GARLIC (GAmma Reconstruction at a LInear Collider exper-

iment) is designed to achieve highly efficient identification of photons within hadronic showers, which mostly come from high energy neutral pion decays. Because the photons from these pions will be highly collimated, this same technique can be used to identify collimated photons from low mass ALP decays. To begin, we examine in Fig. 3.3 the angle between photons from π^0 decays as a function of the π^0 energy and the ECAL radius at the ILD (nominal ECAL radius is 1843mm). The photon reconstruction performance is a function of the Molière radius, which is

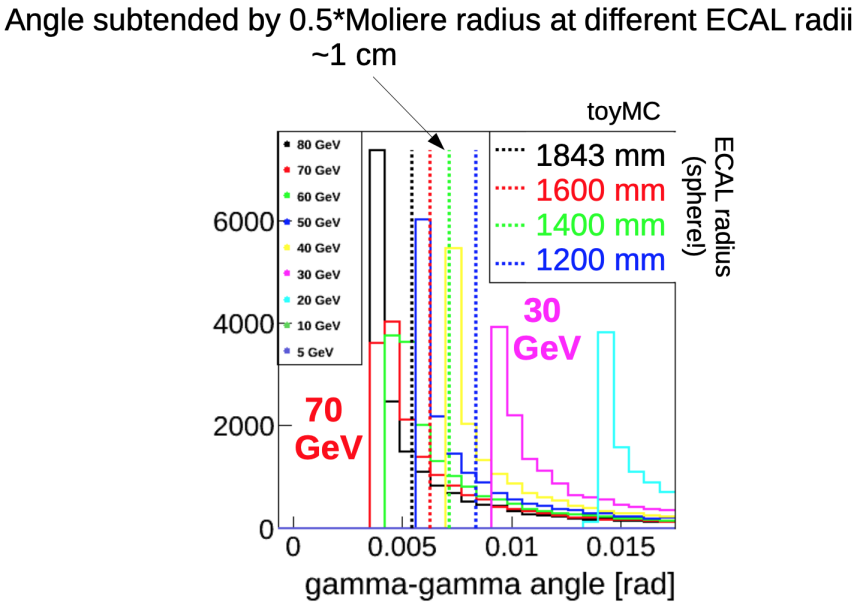

Figure 3.3: Angle between photons from π^0 decays as a function of π^0 energy. Also depicted with dashed lines are the angle subtended by half a Molière radius at different ECAL radii. Figure from [8].

the transverse radius at which a single photon deposits 90% of its energy. The smaller the Molière radius, the more separated each single photon will be. At $E_\pi = 20$ GeV, the Molière radius is roughly half the distance between the pair of photons. At a pion energy of 20 GeV, GARLIC reconstructs 2 photons correctly about 85% of the time.

We would like to adopt this performance to reconstruct photons from low-mass ALP decays. To do so we first need to understand what is the minimum ΔR between photon pairs that we can expect to reconstruct. If we take the results from the 20 GeV pion seriously, the photons from this decay have a peak separation of $\Delta R = 4 \times m_\pi / E_\pi = .027$. We still need to impose separation criteria on the photons. We can again use the pion reconstruction as a test case. Fig. 3.4 shows the fraction of π^0 that have photons separated by greater than 2, 1, 0.5 Molière radii in the ECAL. At the nominal ECAL radius, almost 100% of pions with E = 15 GeV have photons separated by 2 Molière radii. This means that if we form cones around each photon of $\Delta R = 4 \times m_\pi / (15\,\mathrm{GeV}) = .035$ [67], then roughly 10% of the energy inside each cone will be from the

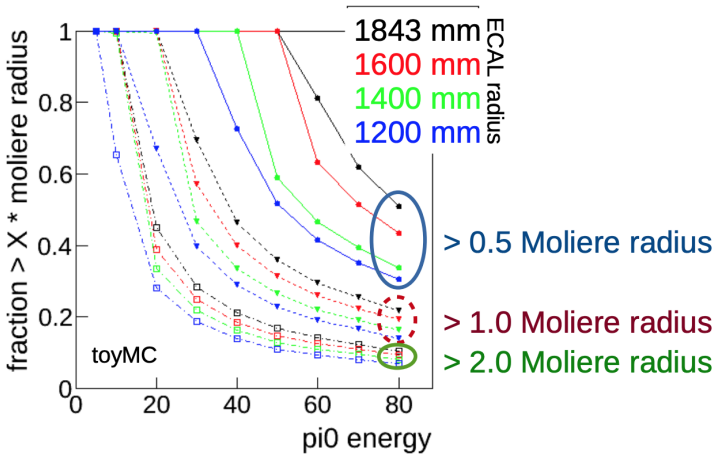

Figure 3.4: Fraction of π^0 that have photons separated by greater than 2, 1, 0.5 Molière radius in the ECAL. Figure from [8].

other photon. Thus we can use this as our photon separation criteria.

We choose to make photons with an isolation cone of $\Delta R = 0.035$, and a $PT_{iso} = 0.1$, meaning that no more than 10% of the PT contained in our cone can come from another photon. The effect of this cut will have on our efficiency to identity photons can be seen from Fig. 3.5 below. For masses below 0.5 GeV, the ΔR between photons can be significantly smaller than 0.035, making photon pair reconstruction challenging. At m_a = 0.5 GeV, the peak of the distribution is near $\Delta R = 0.04$ which allows for sufficient separation for both photons in the pair. We simulated 50,000 $e^+e^- \to a\gamma \to \gamma\gamma\gamma$ events at $\sqrt{s} = m_Z$, for $m_a = 0.5, 1, 2, 3, 6$ GeV. To test our separation criteria we can compute the average number of photons reconstructed. With perfect reconstruction we would expect this to be 3. Failing separation cuts, as well as failing a cut on the minimum photon energy (2 GeV), reduces this number. For $m_a = 0.5$ GeV we reconstruct on average 1.8 photons per event, significantly below 3. This is because quite often the pair of photons from the scalar decay fail separation criteria and thus are rejected. At $m_a = 1$ GeV and above the average number of photons reconstructed is 2.7 due to the much larger ΔR between photon pairs.

3.4 Signal vs. Background

Searches for $Z \to 3\gamma$ have been made difficult because of the relatively large SM background $e^+e^- \to 3\gamma$, which has a cross section at $\sqrt{s} = m_Z$ of approximately 4.1 pb (computed at leading order using MadGraph aMC@NLO [74]). We have not taken into account higher order QED/EW

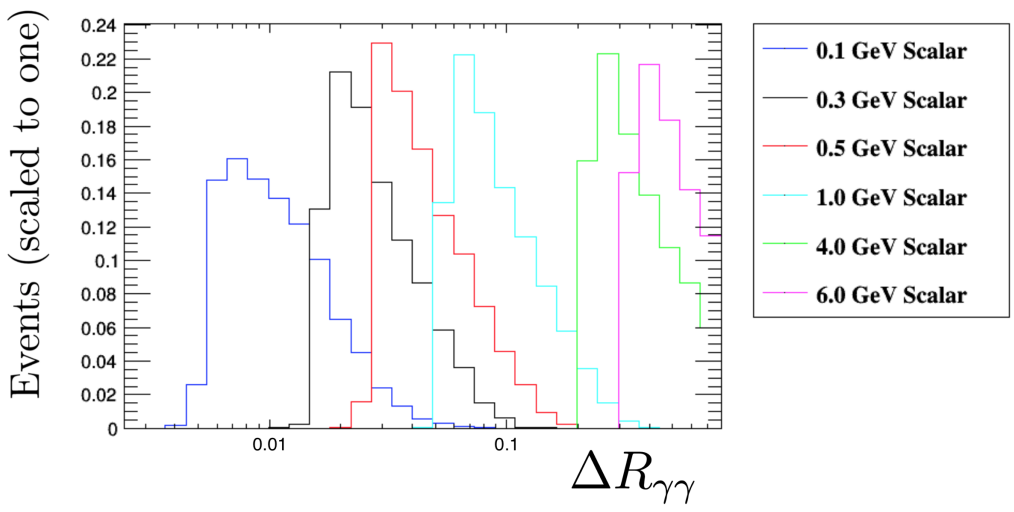

Figure 3.5: ΔR between photons from the ALP decay for a range of ALP masses between 0.1 and 6.0 GeV. The peak of the distribution shifts towards higher ΔR for larger masses, following the form $\Delta R_{\text{peak}} = 4m_a/m_Z$

.

corrections as these tend to be mild except at kinematic extremes [107]. In defining all cross sections we require that each final state photon have $E_\gamma > 2\,\text{GeV}$ and have a pseudorapidity satisfying $\eta < 2.5$.

The tree level $e^+e^- \to Z \to 3\gamma$ cross section in the ALP extension we are considering depends on the mass of the scalar, m_a, and the coupling of the ALP to the hypercharge gauge bosons. We want to investigate the sensitivity to light scalars in this channel. We simulated 100,000 signal events over a range of masses from 0.4 GeV to 50 GeV using our signal model with MadGraph v2.6.7 aMC@NLO [74], showered with Pythia 8.2 [108]. We use the generic ILC Delphes card [109] provided by the ILCSoft developers which simulates the response of a generic ILC detector. We modify the detector cards in accordance with section 3.3. To isolate our signal over the Standard Model background e^+e^- background we need only make a small number of simple cuts. The first is of course that we have three non overlapping, efficiently reconstructable photons. The effect of this cut and its limitations are described in section 3.3. The second cut utilizes kinematic information from the two body, on-shell Z decay. Being a two body decay, the energy of the recoiling photon is a fixed function of m_a, $E^\gamma_{\text{recoil}}(m_a) = (M_Z^2 - m_a^2)/2M_Z$. Thus, when searching for an ALP of mass m_a, one can require that one photon out of the three have an energy near $E^\gamma_{\text{recoil}}(m_a)$. We choose to search for photons within 5 GeV of this energy. These cuts are summarized below.

1. 3 non-overlapping ($\Delta R > .035$) photons with $E_\gamma > 2$ GeV
2. $|E_\gamma - E^\gamma_{\text{recoil}}(m_a)| < 5$ GeV

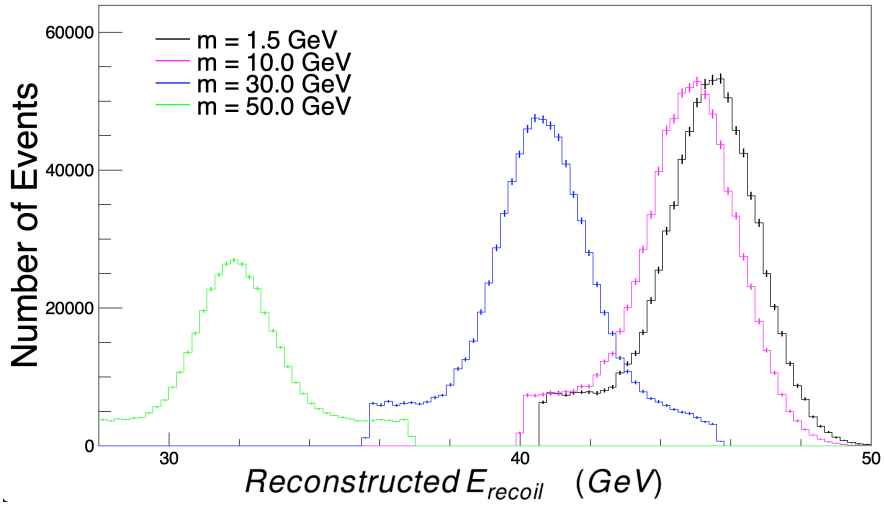

Figure 3.6: Reconstruction recoil photon energy distribution from $Z \to a\gamma$ signal events. For each value of m_a photons are required to have an energy within 5 GeV of $E^{\gamma}_{\text{recoil}}(m_a)$. Each reconstructed distribution is peaked near the true value of $E^{\gamma}_{\text{recoil}}(m_a)$.

For small m_a, $E^{\gamma}_{\text{recoil}}$ is approximately $m_Z/2$. As can be seen in Fig. 3.6, the recoil photon energy cut is especially important for m_a above 30 GeV where the recoil energy starts to decrease significantly from $m_Z/2$. Below in Fig. 3.7 we plot the signal and background yield as a function of m_a with $g_{aBB} = 1\,\text{TeV}^{-1}$. With just the above cuts, the ILC Giga-Z would observe $\mathcal{O}(10^6\,\text{events})$ over the entire range of masses between 0.4 GeV and 50 GeV with only 100 fb^{-1} of integrated luminosity.

It should be noted that while polarization effects are an extremely important part of the ILC run plan, they should be play little role in this search. The SM background for our search is purely QED so polarization has no effect on the background cross section. The signal process involves S-channel production of a Z which is affected, but only changes the signal cross section by a factor of 2 depending on the use of like or oppositely polarized beams. This should not change our estimated limits by much. We can easily examine the sensitivity of the ILC to the above model as the coupling g_{aBB} decreases. For a given coupling, g, producing a signal yield, N, we can find the signal yield, N', with coupling g' simply by using $N' = N(\frac{g'}{g})^2$. To produce an upper limit on g_{aBB} at a 95% confidence level, we can look for when the signal yield, as a function of m_a and g_{aBB}, exceeds two times the uncertainty on the background. Essentially, if the background yield in the signal region for $m_a = m$ GeV is B events, then we can exclude all couplings for an ALP with mass m GeV that produce more than $2 \times \sqrt{B}$ signal events. Doing this for a range of masses gives us the exclusionary power of the ILC Giga-Z program at 95% confidence.

After obtaining the signal and background yields in our mass range of interest, we compute the

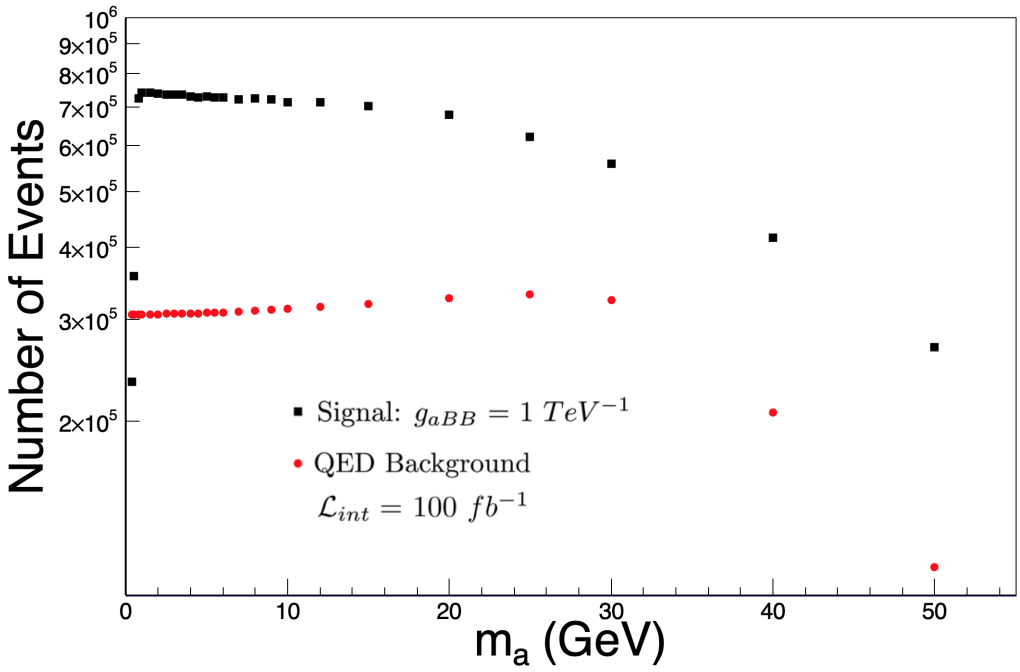

Figure 3.7: Signal and background yields for a range of ALP masses for fixed $g_{aBB} = 1\,\mathrm{TeV}^{-1}$. Yields are normalized to an integrated luminosity of 100 fb^{-1}. Almost 10^6 signal events are expected for this value of g_{aBB}, well above the Standard Model background.

upper limit on g_{aBB}, shown in Fig. 3.8, according to the procedure described above. We include 1σ and 2σ error bars which take into account the statistical uncertainties on the signal yield. Obviously in a real analysis systematic experimental and theoretical uncertainties would have to be taken into account, but we do not expect this to modify our bounds a significant amount. We find that at masses between 0.4 and 50 GeV, the ILC can place stringent upper limits on g_{aBB} which improve on LEP's by over an order of magnitude. To compare against current bounds we plot in Fig. 3.9 the ILC Giga-Z exclusion region along with current constraints, as a function of $g_{aBB}\,(\mathrm{TeV}^{-1})$. We would like to stress that this simple analysis, based only on the granularity of the future ILC detectors and the kinematics expected from the $Z \to a\gamma$ decay, is able to probe much more deeply new regions of parameter space in this model. A more sophisticated experimental analysis would involve a bump-hunt search on the invariant mass of the two photon system from the ALP decay. Additional information which could be used to make these bounds even stronger could be obtained from the angular separation between the photons from the ALP decay. For $m_a < 20$ GeV, the distribution of ΔR of these two photons is peaked at low values (see Fig. 3.5), while the background distribution falls quickly in this region. Utilizing the excellent angular separation abilities of the ILC detectors, one could require that this two photon system be below a particular angular separation, further reducing the background. Combining this kinematic information and bump hunt search using machine learning techniques such as a Boosted Decision Tree or TMVA could greatly increase the search power of this analysis. Finally, for very small

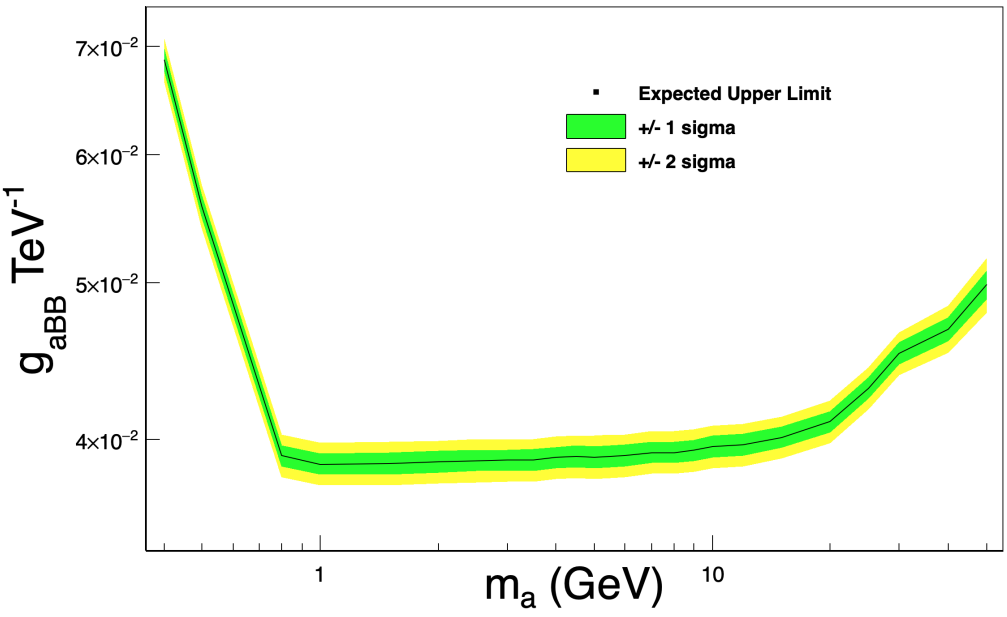

Figure 3.8: Upper limit on g_{aBB} over the range of masses 0.4 to 50 GeV. 1σ and 2σ error bars are shown in yellow and green.

masses ($< 0.5\,\mathrm{GeV}$), the two photons from the ALP decay would be collimated enough as to overlap in the detector and possibly be registered as a single photon.Thus, a straightforward two photon analysis, or one which uses shower shape variables to discriminate overlapping photons from single photons could strengthen bounds in the low mass region.

3.5 Conclusion

Axion-Like Particles (ALPs) represent an exciting and generic, calculable SM extension, with a parameter space that is being investigated through many different fronts. We have shown that even small ($\mathcal{O}(10^{-2}\,\mathrm{TeV}^{-1})$) ALP couplings to hypercharge generate a significant number of signal events at an experiment like the ILC over a range of masses from 0.4 GeV to 50 GeV. The exceptional photon reconstruction abilities of the future ILC detector(s) will allow for efficient identification of 3 photon events even at very small photon separations. This represents an exciting opportunity for the ILC to probe new light, weakly coupled physics which interacts with the Z and to make a discovery.

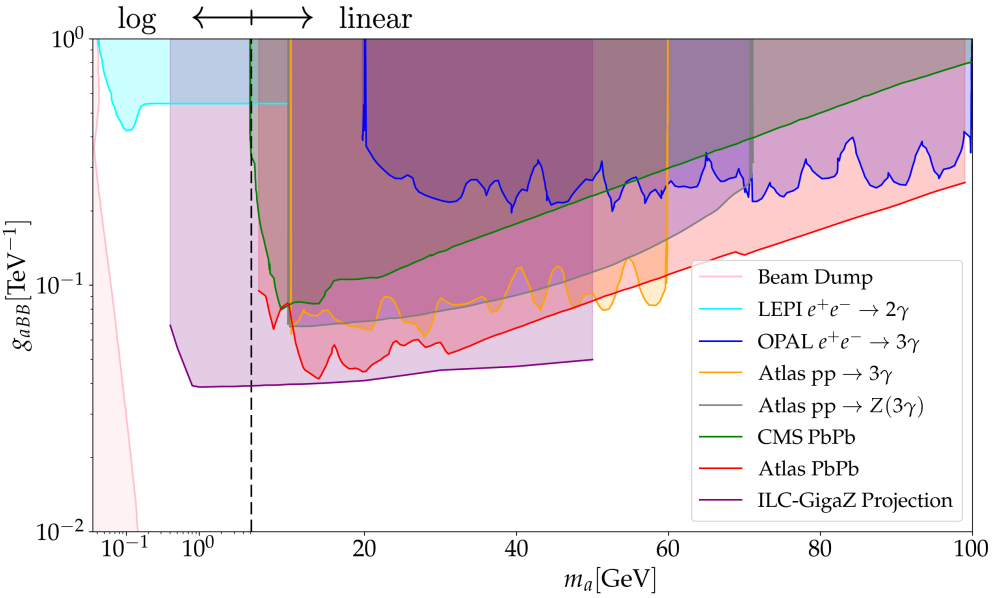

Figure 3.9: ILC Giga-Z exclusion region against past experiments exclusion regions. We plot the limit here as a function of g_{aBB} (TeV^{-1}) The ILC will significantly improve limits from over the whole range of masses from 0.4 to 50 GeV.

Chapter 4

Discovering Axion-Like Particles with Photon Fusion at the ILC

Abstract: Experimental searches for Axion-Like Particles (ALPs) which couple to the electroweak bosons span over a wide range of ALP masses, from MeV searches at beam-dump experiments, to TeV searches at the LHC. Here we examine an interesting range of parameter space in which the ALP couples only to hypercharge. In the GeV to hundreds of GeV mass range, the contribution of an ALP to light by light scattering can be significant. By making simple kinematic cuts, we show that the ILC running at $\sqrt{s} = 250\,\mathrm{GeV}$ or $\sqrt{s} = 500\,\mathrm{GeV}$ can discover ALPs in this range of masses with significantly smaller couplings to the SM than previous experiments, down to $g_{aBB} = 10^{-3}\,\mathrm{TeV}^{-1}$.

4.1 Introduction

As the production and decay of an ALP in this model is a purely electroweak process, we will show that the ILC, a next generation e^+e^- collider, is the ideal laboratory to discover and study ALPs with electroweak scale masses. In Chapter 3 I introduced a model of Axion-Like Particles which couple purely to hypercharge. After electroweak symmetry breaking this coupling induces couplings of the ALP to pairs of photons, Z bosons, and photon-Z pairs. We saw that the ILC Giga-Z program could place powerful constraints on ALPs in the 5-50 GeV range, filling in a significant gap of coverage in this sub-weak scale mass range. In addition to probing this range of ALP masses, the couplings of the ALP to pairs of photons can be leveraged to probe much larger ALP masses via the ALPs contribution to light by light scattering. I show that the by using the ILC running in the 250 GeV or 500 GeV mode as a photon collider, the ILC can probe much larger ALP masses, up to 350 GeV for the ILC500, strengthening the constraints on this model by more than an order of magnitude.

4.2 ALP Production and constraints

The most promising search channel for heavy ($m_a > 100\,\mathrm{MeV}$) ALPs coupled to hypercharge depends strongly on the collider type. In [4, 5, 7], ALPs with couplings to photons were searched for in Ultra-Peripheral Lead-Lead ion collisions at CMS and ATLAS. Here the process of interest is $\mathrm{PbPb} \to \gamma\gamma\mathrm{PbPb}$ where quasi-real photons from two incoming lead ions scatter from each other at large impact parameter, leaving the lead ions intact. These analyses take advantage of the Z^4 enhancement in coherent photon-photon luminosity, enhancing the discovery sensitivity for low mass (5 - 100 GeV) scalars and pseudo-scalars which couple to photons, even with the reduced PbPb luminosity (only $1\,\mathrm{nb}^{-1}/\mathrm{year}$). The coherent enhancement becomes suppressed past $\gamma\gamma$ invariant masses of $\approx$ 200 GeV (as nuclear breakup becomes more probable), limiting the mass reach of this method. Similar analyses are possible in $p-p$ collisions ($pp \to p\gamma\gamma p$), though the intact protons must be forward tagged to overcome the large hadronic backgrounds at the LHC [112].

Other non-exclusive $\gamma\gamma$ final states can been used to search for ALPs, such as in vector boson fusion [110] where the back to back jets from the partonic process as well as the two final state photons are used for triggering. This gives competitive constraints in the 10 MeV to 100 GeV range with ALP couplings down to $0.5\,\mathrm{TeV}^{-1}$. Finally in the high mass region $200\,\mathrm{GeV} < \mathrm{m_a} < 2.6\,\mathrm{TeV}$, ATLAS searches for spin 0 resonances in diphoton final states [**?**] have been re-interpreted by employing photon distribution functions in the proton to produce the most stringent constraints at these high masses [97].

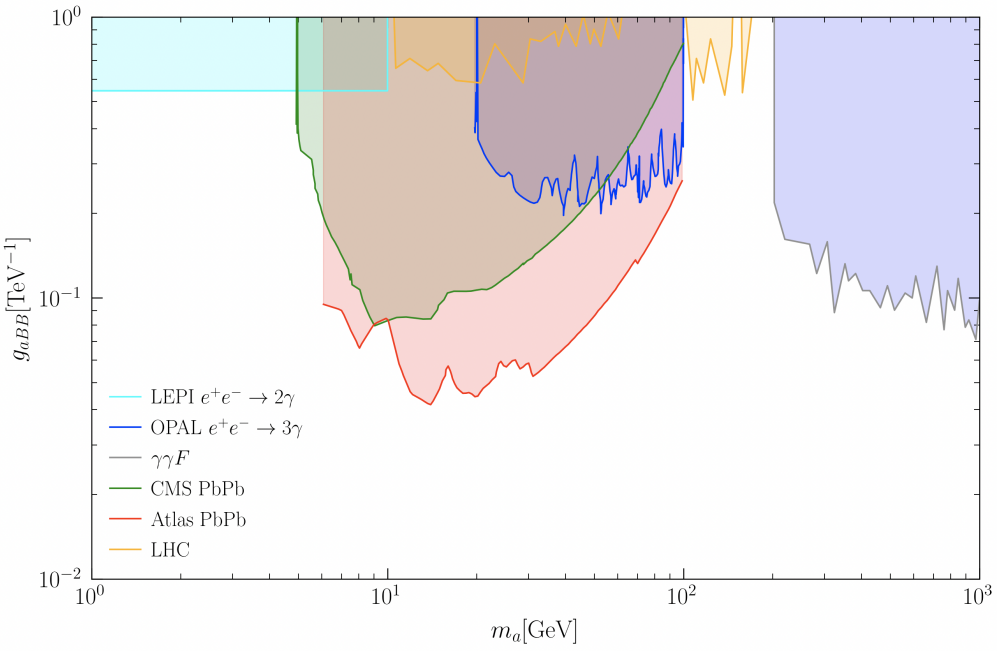

Figure 4.1: Summary of constraints on ALPs coupled to hypercharge. Figure adapted from [3]

A summary of these constraints on g_{aBB} is given in Fig. 4.1. As one can see, couplings at the $10^{-1}\,\mathrm{TeV}^{-1}$ level are currently being probed depending on the mass range of interest, with the strongest constraints between 10 and 100 GeV, and above 200 GeV, with a curious gap in sensitivity in the 100 - 200 GeV region. In this region (and at even smaller values of m_a) we will show that the ILC running at either 250 GeV or 500 GeV will increase the sensitivity to this model between 10 and 200 GeV, and to even higher masses at ILC500. In the next section we briefly review the capabilities of the ILC.

4.3 ILC

The International Linear Collider (ILC) is a proposed next generation e^+e^- collider [104]. The ILC hopes to study the Standard Model (SM) with unprecedented precision at several center of mass energies including $\sqrt{s} = m_Z,\ 250\,\mathrm{GeV},\ 500\,\mathrm{GeV}$ and possibly $1\,\mathrm{TeV}$, with a particularly close eye on precision electroweak and Higgs physics. Besides testing the SM, the ILC also has unique capabilities to search for Beyond the SM (BSM) physics. Currently the proposed run plan for the ILC is to collect $2\,\mathrm{ab}^{-1}$ at 250 GeV and $3\,\mathrm{ab}^{-1}$ at 500 GeV center of mass. Obviously these integrated luminosities are preliminary but we would like to stress that the reach of this specific BSM model is highly dependent on the integrated luminosity collected at each center of mass energy. Combining these large luminosities with a clean collision environment mostly free of the strong interactions which challenge the LHC make the ILC an excellent laboratory to

search for rare, new physics. Additionally, the ILC's highly granular detectors allow for excellent photon identification and isolation, allowing photons with very small separations from each other to be identified, which is crucial for searching for low mass particles which decay to pairs of photons. Information on the two main proposals for ILC detectors, the ILD and the SiD can be found in [**?**, **?**].

4.4 Equivalent Photon Approximation (EPA)

The ILC, in addition to being an e^+e^- collider, is also a $\gamma\gamma$ collider, by virtue of the equivalent photon approximation [113]. In the EPA, photons with small virtuality are emitted via bremstrahlung almost collinearely with an incoming lepton beam, such that $Q^2 = -q^2 \approx 0$, and the photons can be treated as real. Cross sections are computed by using these almost real photons as the incoming particles in the hard scattering process, and then convolving this cross section with the photon luminosity function.

In more detail, the cross section for the production of a state X is given in the EPA by

$$\sigma(e^+e^- \to e^+e^- X)(s) = \int ds_{\gamma\gamma} \frac{d\mathcal{L}(s_{\gamma\gamma})}{ds_{\gamma\gamma}} \sigma(\gamma\gamma \to X, s_{\gamma\gamma}), \tag{4.4.1}$$

where, $\sqrt{s}$ is the center of mass energy of the lepton beams and $\sqrt{s_{\gamma\gamma}}$ is the invariant mass of the interacting photon pair. The approximation is accurate up to corrections of order $Q^2/s_{\gamma\gamma}$ where $Q^2 = -q^2$ is the virtuality of the radiated photons, so the approximation accuracy increases as we consider larger values of $s_{\gamma\gamma}$. In the EPA, the photon luminosity function $\mathcal{L}(s_{\gamma\gamma})$ can be computed as

$$\frac{d\mathcal{L}(s_{\gamma\gamma})}{ds_{\gamma\gamma}} = \frac{1}{s} \int \frac{N(x_1)}{x_1} N(x_2 = s_{\gamma\gamma}/x_1 s) dx_1. \tag{4.4.2}$$

Here $N(x)$ is the Weizsacker-Williams photon spectrum which gives the distribution of photons emitted as a function of the energy fraction, $x = (E_e - E_e^{'})/E_e = E_\gamma/E_e$, and $x_1(x_2)$ is the fraction of the $e^-(e^+)$ energy carried by the incoming photon.

$$N(x) = \frac{\alpha}{2\pi} \left((1 + (1-x)^2) \log \left(\frac{Q^2_{\max}}{Q^2_{\min}} \right) - 2m_e^2 x^2 \left(\frac{1}{Q^2_{\min}} - \frac{1}{Q^2_{\max}} \right) \right). \tag{4.4.3}$$

In Eq. 4.4.2, $Q^2_{max(min)}$ is the maximum (minimum) virtuality of the EPA photons. We take $Q^2_{min} = m_e^2 x^2/(1-x)$ and $Q^2_{max} = 2\,\mathrm{GeV}^2$. In the center of momentum frame of the $\gamma\gamma$ system, $s_{\gamma\gamma} = x_1 x_2 s$. This relationship fixes x_2 as a function of $s_{\gamma\gamma}$ and x_1.

We use MadGraph5_aMC@NLO [114] to simulate this process at the ILC by selecting the hard

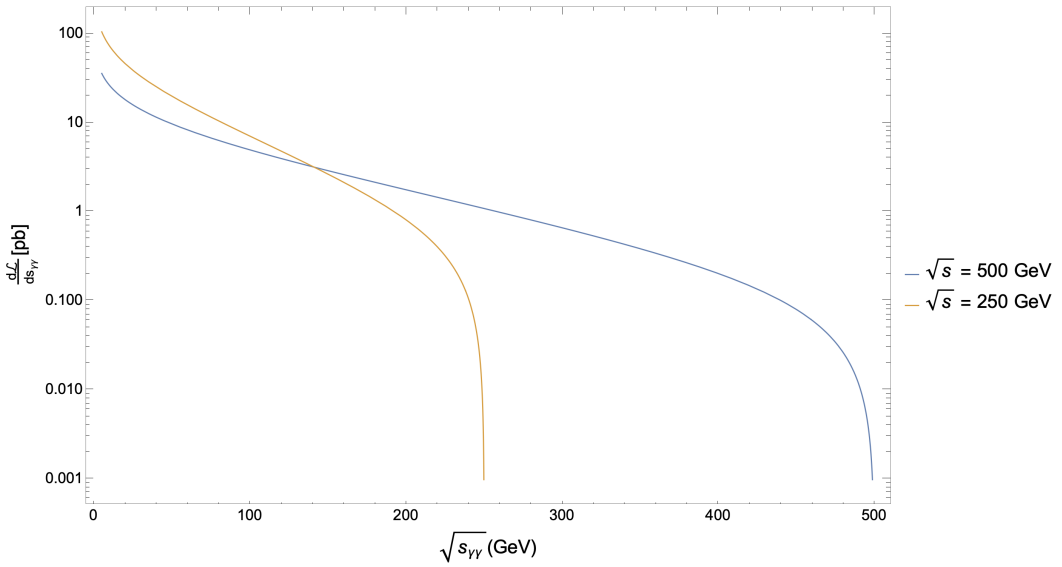

Figure 4.2: Photon Luminosity, $\frac{d\mathcal{L}}{d\sqrt{s_{\gamma\gamma}}}$, for both ILC250 and ILC500. The $\gamma\gamma$ luminosity steeply falls as $s_{\gamma\gamma}$ increases, dropping to 0 when $s_{\gamma\gamma}$ approaches s. Note the logarithmic y axis.

$\gamma\gamma \rightarrow \gamma\gamma$ process and choosing the "photons from electrons" beam mode. This selects EPA photons as the incoming particles from a lepton beam with center of mass energy, $\sqrt{s}$, chosen by the user. This process is pictured in Fig. 4.3.

It is interesting to note that even though the ILC nominal run plan includes significant beam time with polarized leptons, this has little effect on the EPA cross section. The effect of the polarization of an incoming lepton on the polarization of an outgoing EPA photon is of order $x = E_\gamma/E_l$, so that only for $x \approx 1$ are the photons fully polarized. For small values of x the photon is effectively unpolarized [115]. To validate MadGraph's implementation of the EPA, we have verified that the numerical predictions for the production of e^+e^- pairs via photon fusion match our analytical calculations for the same process. This ensures the accuracy of MadGraph's calculation of the photon luminosity function.

The photon luminosity for both ILC250 and ILC500 is shown in Fig. 4.2. Note the steep decrease in luminosity as $s_{\gamma\gamma}$ increases, with the photon luminosity for ILC250 dropping to 0 at $\sqrt{s_{\gamma\gamma}} = 250\,\mathrm{GeV}$. Events are showered using Pythia8 [108] and run through a fast detector simulation implementation of a generic ILC detector using Delphes [109, 116]

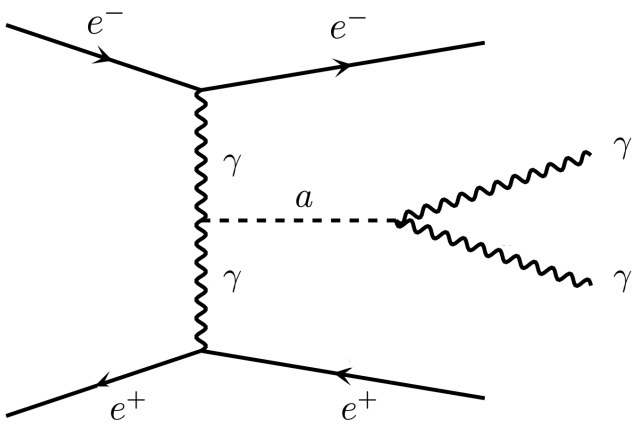

Figure 4.3: ALP production via photon fusion from EPA photons and subsequent decay into a pair of photons. Only s channel contribution is shown.

4.5 Backgrounds and Signal Selection

The signal selection criteria for this model is two isolated photons with no other activity and the recoiling electrons undetected. For our signal model several benchmark ALP masses were chosen based on running at $\sqrt{s} = 250$ GeV or $\sqrt{s} = 500$ GeV, as larger invariant photon masses can be reached in the later stage. For $\sqrt{s} = 250$ GeV ALP masses are chosen from 5 - 150 GeV in steps of 2 GeV, and for $\sqrt{s} = 500$ GeV ALP masses from 5 - 350 GeV were chosen with the same step size.

For simulations we chose an ALP-hypercharge coupling, g_{aBB}, with value $10^{-3}\,\mathrm{GeV}^{-1}$. In searching for this signal, several background processes must be suppressed. The first and most obvious background is ordinary SM light by light (LBL) scattering, which was first observed by ATLAS in ultra peripheral PbPb collisions [117]. We simulated this process at 1-loop level in MadGraph using the $\mathrm{sm\_loop\_qed\_qcd\_Gmu}$ model file with all default parameters, generating 400,000 events [118]. This process can be most efficiently suppressed via an invariant mass cut on the two final state photons, as the SM LBL $m_{\gamma\gamma}$ peaks at small values and exponentially falls off at higher values of $m_{\gamma\gamma}$. This can be seen in Fig. 4.4, where we plot the invariant mass distribution of the final state photons for SM LBL scattering and our ALP signal, with $m_a = 35$ GeV.

Another interesting background is $e^+e^- \to Z\gamma\gamma \to \bar{\nu}_l\nu_l\gamma\gamma$ with the neutrinos escaping undetected. This background can be suppressed via a cut on the transverse momentum of photon system, $\mathrm{PT}_{\gamma\gamma} < 5$ GeV, which is equivalent to a cut on missing transverse energy. As can be seen in Fig. 4.5, the $Z\gamma\gamma$ background can be efficiently suppressed with very little effect on the

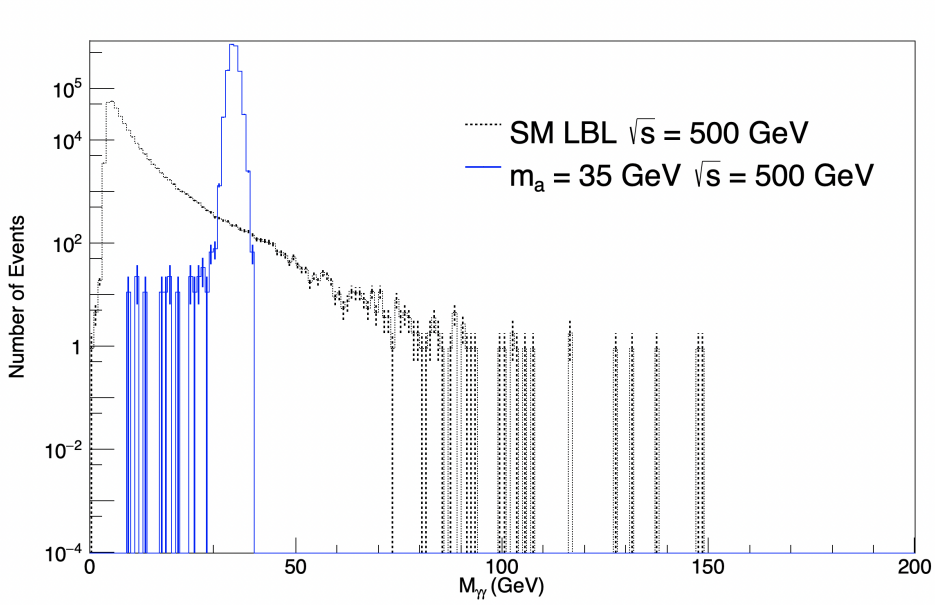

Figure 4.4: Invariant mass distribution of the $\gamma\gamma$ system at ILC with $\sqrt{s} = 500$ GeV. Shown in blue solid line is the distribution from an ALP with $m_a = 35$ GeV and $g_{aBB} = 10^{-3}$ GeV, and the SM LBL distribution in dotted black.

ALP signal. Additionally we require that the pseudorapidity of each final state photon satisfies $\eta_\gamma < 2.4$. With these selection cuts, the ILC running at $\sqrt{s} = 500\,\mathrm{GeV}(\sqrt{s} = 250\,\mathrm{GeV})$ with an integraed luminosity of $2\,\mathrm{ab}^{-1}$ could produce as many as 240(160) ALPs with a mass of $35\,\mathrm{GeV}$ with coupling $g_{aBB} = 10^{-4}\,\mathrm{GeV}^{-1} = 10^{-1}\,\mathrm{TeV}^{-1}$.

4.6 Discovery reach of the ILC

To compute the reach of the ILC in the m_a, g_{aBB} plane, we utilize the exact Asimov significance, Z^A, for exclusion [119]. Consider signal and background processes with poisson means s and b respectively. The p-value for exclusion of the signal model if n events are observed is given by

$$p_{\mathrm{excl}}(n, b, s) = \sum_{k=0}^{n} P(k|s+b) = Q(n+1, s+b) = \frac{\Gamma(n+1, s+b)}{\Gamma(n+1)}, \tag{4.6.1}$$

where $Q(a, x) = \Gamma(a, x)/\Gamma(a)$ is the regularized upper incomplete gamma function [120]. In computing the exact Asimov significance the exact p-value for exclusion is used with the number of events n replaced by its expected mean, which for exclusion is simply the mean number of background events b. This leads to the following expression for the exclusion p-value

$$p_{\mathrm{excl}}^{\mathrm{Asimov}} = Q(b+1, s+b). \tag{4.6.2}$$

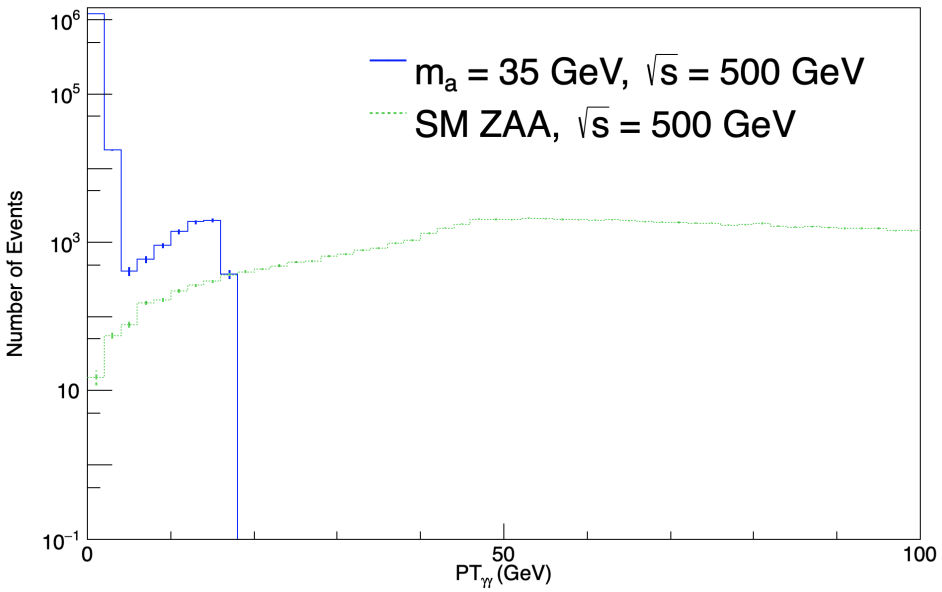

Figure 4.5: $\mathrm{PT}_{\gamma\gamma}$ distribution at ILC with $\sqrt{s} = 500\,\mathrm{GeV}$. Shown in blue solid line is the distribution from an ALP with $m_a = 35\,\mathrm{GeV}$ and $g_{aBB} = 10^{-3}\,\mathrm{GeV}$. The $Z\gamma\gamma$ distribution is the dotted green line.

The exact Asimov significance computed in this way is a more conservative estimate of the exclusion significance and does not suffer from the counter-intuitive flaws of the median significance as noted in [119].

At each ALP mass we compute the expected number of background events, b, given the cuts discussed above. We then invert $Q(b+1, s+b) = 0.05$ to compute the number of signal events which gives us our 95% confidence limit on the ALP coupling. Note that this is always well defined because the upper incomplete gamma function is monotonic. Finally, we translate the number of signal events into an expected upper limit on g_{aBB}. Note that in extracting limits on g_{aBB} we use the narrow width approximation where

$$\sigma(\gamma\gamma \to a \to \gamma\gamma) \propto \sigma(\gamma\gamma \to a) \times \mathrm{BR}(\mathrm{a} \to \gamma\gamma) \propto \mathrm{g}^2_{\mathrm{aBB}}, \tag{4.6.3}$$

which is valid for all masses and couplings considered here. To compare against similar existing experimental bounds, we plot the projected upper limits on g_{aBB} as a function of ALP mass against bounds from other past and current experiments in Fig. 4.6.

At first glance it is easy to see that running this search at $\sqrt{s} = 500\,\mathrm{GeV}$ gives access to much higher ALP masses due to the larger energy available from each incoming lepton. At ILC500, ALPs with masses of almost 350 GeV can be produced while having a feeble coupling to hypercharge of almost $10^{-3}\,\mathrm{TeV}^{-1}$. In contrast ILC250 is limited to ALP masses below 150 GeV with

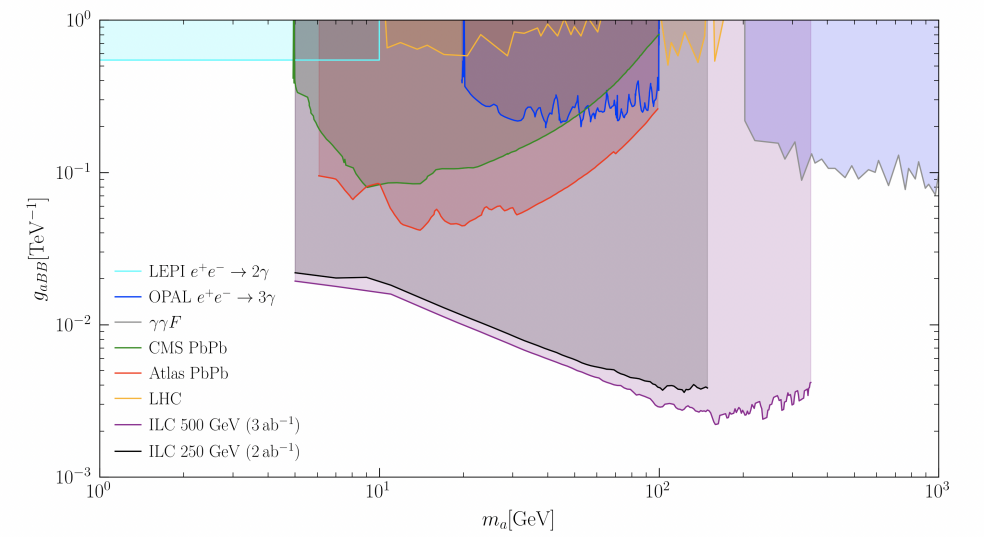

Figure 4.6: ILC500 (purple) and ILC250 (black) reach as a function of m_a. The ILC250 will significantly open up new discovery territory in the 50 - 150 GeV region with the ILC500 improving this capability up to masses of 350 GeV.

similar values of g_{aBB}. It is interesting to note that nowhere in this m_a, g_{aBB} region does ILC250 outperform ILC500. This is due to a complicated interplay between the ALP production cross section as well as the photon flux which is itself a function of the center of mass energy of the lepton beams. Suffice to say that ILC500 has significantly better discovery capabilities for ALPs in this mass range.

4.7 Conclusion

We have shown that photon-photon scattering mediated by an ALP can be a powerful probe of Axion-Like Particles with couplings to hypercharge. Using simple kinematic cuts as well as taking advantage of the relatively background free nature of this signal leads to a powerful search strategy for these particles. Additionally, this improves the physics case for the ILC and other e^+e^- colliders, showing that the clean and highly controlled collider environment provides excellent access to weakly coupled new physics.

Chapter 5

Conclusion

In this thesis I have defined the Standard Model as it stands today, and highlighted several deep-seated experimental and theoretical issues. These challenges must be met with new theoretical ideas spanning the landscape of BSM theories. We have investigated some general extensions of the Standard Model involving singlet scalars and Axion-Like Particles and showed that if these new particles couple to photons that they may leave striking signatures in current and future experiments. At the LHC, including ξ-jets in the searches for the Higgs could dramatically increase the ability of the LHC to search for light scalars coupled to the Higgs as in Chapter 2. In Chapters 3 and 4 I examined a model of an Axion-Like Particle coupled to hypercharge which is amenable to discovery at the ILC. In particular, I have highlighted the complementarity of the ILC Giga-Z with the higher energy 250 and 500 GeV ILC run plans, allowing the ILC to have incredible sensitivity to this model across a range of masses from 5 to 350 GeV. It remains the work of future theorists and experimentalists to set out and discover or rule out such theories.

APPENDIX A

Feynman Rules for ALP Model Coupled to Hypercharge

A.1 Axion-Like Particles Coupled to Hypercharge

The Lagrangian for an Axion-Like Particle (ALP) coupled to hypercharge is given by

$$\mathcal{L} = \mathcal{L}_{SM} + \frac{1}{2}(\partial_\mu a)(\partial^\mu a) - \frac{m_a^2}{2}a^2 - \frac{g_{aBB}}{4}aB_{\mu\nu}\tilde{B}^{\mu\nu} \tag{A.1.1}$$

where $\tilde{B}^{\mu\nu} = \frac{\varepsilon^{\mu\nu\rho\sigma}B_{\rho\sigma}}{2}$, and $\varepsilon_{\mu\nu\rho\sigma}$ is the totally antisymmetry tensor in 4 dimensions. After EW symmetry breaking this Lagrangian leads to couplings of the ALP to the photon and Z with the following Feynman rules:

- $a\gamma\gamma$: $2ig_{aBB}c_w^2\varepsilon_{\mu\nu\rho\sigma}(p_{\gamma_2}^\rho p_{\gamma_1}^\sigma - p_{\gamma_1}^\rho p_{\gamma_2}^\sigma)$
- $aZ\gamma$: $-2ig_{aBB}c_w s_w\varepsilon_{\mu\nu\rho\sigma}(p_Z^\rho p_\gamma^\sigma - p_\gamma^\rho p_Z^\sigma)$
- aZZ: $2ig_{aBB}s_w^2\varepsilon_{\mu\nu\rho\sigma}(p_{Z_2}^\rho p_{Z_1}^\sigma - p_{Z_1}^\rho p_{Z_2}^\sigma)$

As a result of the above Feynman rules, an ALP can decay into a pair VV' with $V = (\gamma, Z)$ depending on the mass of the ALP. Below we plot that branching ratio of the ALP into pairs VV' as a function of the ALP mass m_a. Note that we have neglected off shell decays $(a \to V * V')$ as these do not significantly change the branching ratios.

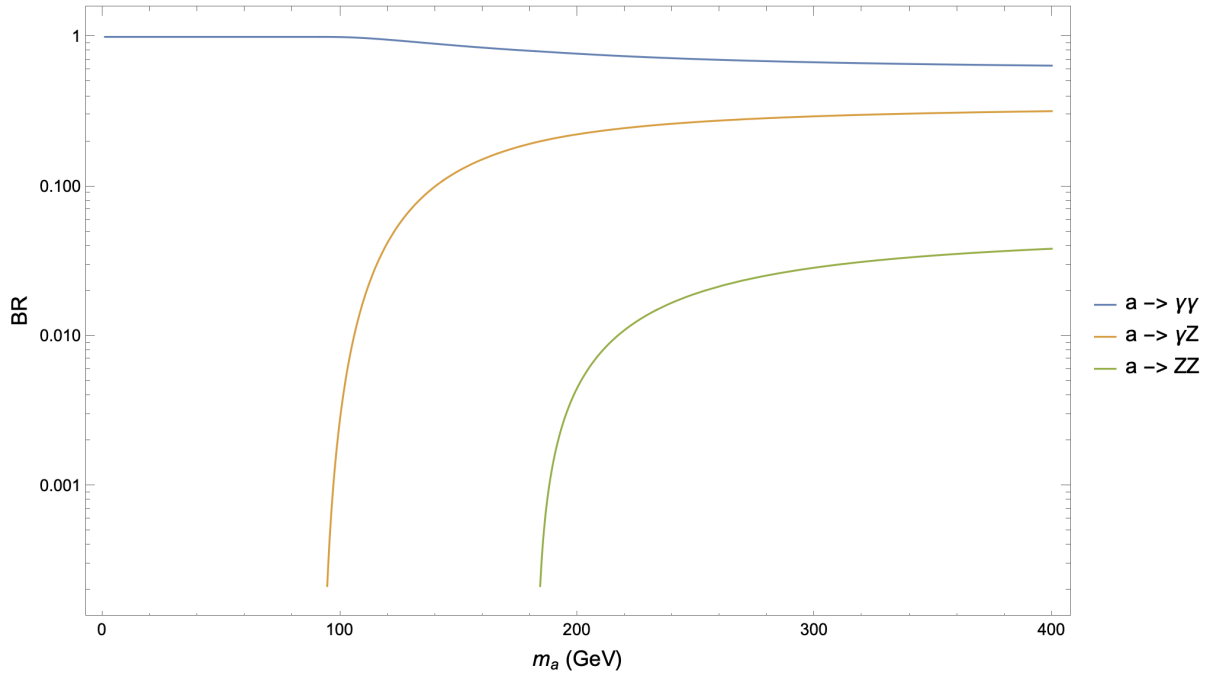

Figure A.1: ALP branching ratio as a function of m_a for the three different tree level decay modes. Note that off shell decays are not included.

APPENDIX B

High Energy Physics Computational Tools

B.1 Summary of Computational Tools

This work relied heavily on several computational tools to calculate Feynman rules and amplitudes, numerically compute cross sections, and evaluate detector efficiencies.

B.1.1 Feynrules and Feyncalc

Feynrules [121] is a Mathematica package that computes Feynman rules for any QFT once the user provides an associated Lagrangian as well as information on the particle content (spin, gauge symmetries, etc.) of the model. Many Feynrules model files exist in the literature already, for both the SM and a variety of BSM theories. These Feynman rules can be taken by the user or be exported into MonteCarlo generators for event production.

In a similar vein, Feyncalc [122] is an extraordinary tool for the symbolic evaluation of Feynman diagrams. Feyncalc can evaluate both tree and loop level diagrams, properly treat Lorentz, and any other index contraction, manipulate Dirac matrices, and do Tensor reduction of integrals.

B.1.2 MadGraph

MadGraph_aMC@NLO [74] is a collection of programs for the automatic computation of tree level and NLO cross sections, and their matching to parton shower programs. The motivation behind the construction of MadGraph is to automate the process of the perturbative expansion of an observable at leading and next to leading order. This is possible at tree and one-loop level because of a universal formalism for curing these observables of infrared divergences, and an automated technique for the evaluation of one-loop amplitudes. Thus, once this general framework is set up, observables for any theory can be computed automatically.

The user instructs MadGraph what model they would like to use by providing a file in the Universal FeynRules Output (UFO) format. These files are produced by Feynrules and contain all particles, interactions, and the specific parameters (masses, couplings, etc.) for that model. Given a model, the user can specify the specific process they would like to investigate. Initial state partons (quarks, leptons) can be used as well as composite particles (protons, ions) as long as the associated pdfs or form factors are provided. In this way the user can compute scattering cross sections at a myriad of different experiments whether they be lepton or proton colliders.

The user has options of defining phase space cuts on the process, such as minimum separation between leptons or jets, or a maximum invariant mass of a pair of particles. In this way one can replicated experimental cuts.

B.1.3 Delphes

Delphes [77] is a fast detector simulation program designed to provide a realistic experimental environment in which to simulate detector response for both SM and BSM phsyics. The Delphes program is modular, based on a typical collider experiment design, a cylindrical volume in which particles propagate through a magnetic field, and each detector contains an electromagnetic calorimeter (ECAL), hadronic calorimeter (HCAL), and muon tracking system. Each detector component is characterized by its detection efficiency and energy resolution, broken down by particle type.

An essential role of these simulations is particle-flow reconstruction, which maximizes the amount of information provided by the various sub-detectors. The end result of this philosophy is a set of particle-flow tracks, containing charged particles, and particle-flow towers, which contain a combination of neutral particles, charged particles with no track, and additional excess deposits. These towers are composed of ECAL and HCAL cells which have energy depositions above some minimum threshold amount set by the user. These outputs serve later as inputs for object identification and jet reconstruction.

APPENDIX C

Equivalent Photon Approximation

C.1 Equivalent Photon Approximation

The Equivalent Photon Approximation (EPA) is used to simplify processes where a charged particle interacts with a system X via the exchange of a photon.

Let us assume that we have an incoming electron and system X, which scatter via the exchange of a virtual photon with momentum q. In the final state we have an electron and a new system Y whose details are unimportant. The photon propagator, $-ig^{\mu\nu}/q^2$ is obviously dominated by the region near $q^2 = 0$.

Without loss of generality, the incident electron momentum can be written as $p = (p, 0, 0, p)$, and the photon and scattered electron momenta as $q \approx (zp, p_T, 0, zp - p_T^2/2zp)$, $k \approx ((1-z)p, -p_T, 0, (1-z)p + p_T^2/2zp)$. These four vectors are all null up to terms of order p_T^4.

Without approximation, the cross section for this process is given by

$$\sigma = \frac{1}{(1+v_X)2p2E_X}\int\frac{d^3k}{(2\pi^3)}\frac{1}{2k^0}\int d\Pi_Y[\frac{1}{2}\Sigma|\mathcal{M}|^2](\frac{1}{q^2})^2|\mathcal{M}_{\gamma X}|^2, \tag{C.1.1}$$

where v_X is the velocity of X. Rewriting the differential $d^3k = \pi dp_T^2 pdz$ and subbing in k^0 and q^2 from the above gives the cross section

$$\begin{aligned}\sigma &= \int\frac{pdzdp_T^2}{16\pi^2(1-z)p}[\frac{1}{2}\Sigma|\mathcal{M}^2|]\frac{(1-z)^2}{p_T^4}\frac{z}{(1+v_X)2zp2E_X}\int d\Pi_Y|\mathcal{M}_{\gamma X}|^2 \\ &= \int\frac{dzdp_T^2}{16\pi^2(1-z)}[\frac{1}{2}\Sigma|\mathcal{M}^2|]\frac{z(1-z)^2}{p_T^4}\sigma(\gamma X\to Y)\end{aligned} \tag{C.1.2}$$

The spin averaged electron emission matrix element, $\frac{1}{2}\Sigma|\mathcal{M}|^2 = \frac{2e^2p_T^2}{z(1-z)}\frac{1+(1-z)^2}{z}$ can be found

in [123]. Inserting this into our total cross section gives

$$\begin{aligned}\sigma &= \int \frac{dzdp_T^2}{16\pi^2}\frac{z(1-z)}{p_T^4}\frac{2e^2p_T^2}{z(1-z)}\frac{1+(1-z)^2}{z}\sigma(\gamma X \to Y) \\ &= \int_0^1 dz \int \frac{dp_T^2}{p_T^2}\frac{\alpha}{2\pi}\frac{1+(1-z)^2}{z}\sigma(\gamma X \to Y).\end{aligned} \tag{C.1.3}$$

We can compute the integral over p_T^2 by integrating over momentum transfers from m_e^2 to s, where s is the squared center of mass energy. This gives the Weizsacker-Williams distribution function which when multiplied by the partonic cross section $\sigma(\gamma X \to Y)$ and integrated over gives the Equivalent Photon Approximation.

$$f_\gamma(z) = \frac{\alpha}{2\pi}\log\frac{\mathrm{s}}{\mathrm{m_e^2}}\frac{1+(1-\mathrm{z})^2}{\mathrm{z}} \tag{C.1.4}$$

The above formula gives the probability of finding a photon of longitudinal fraction z inside the incident electron and is the starting point for the Equivalent Photon Approximation. Further corrections to this formula, including taking into account small virtuality of the photon lead to improved formulas as given in the main text of this thesis.

Bibliography

[1] "A combination of measurements of Higgs boson production and decay using up to 139 fb^{-1} of proton–proton collision data at $\sqrt{s} = 13$ TeV collected with the ATLAS experiment," 8 2020.

[2] de Florian, D. et al., "Handbook of LHC Higgs Cross Sections: 4. Deciphering the Nature of the Higgs Sector," Vol. 2/2017, 10 2016.

[3] Jaeckel, J. and Spannowsky, M., "Probing MeV to 90 GeV axion-like particles with LEP and LHC," *Phys. Lett. B*, Vol. 753, 2016, pp. 482–487.

[4] Sirunyan, A. M. et al., "Evidence for light-by-light scattering and searches for axion-like particles in ultraperipheral PbPb collisions at $\sqrt{s_{\mathrm{NN}}} = 5.02$ TeV," *Phys. Lett. B*, Vol. 797, 2019, pp. 134826.

[5] Aad, G. et al., "Measurement of light-by-light scattering and search for axion-like particles with 2.2 nb^{-1} of Pb+Pb data with the ATLAS detector," 8 2020.

[6] Aad, G. et al., "Search for new phenomena in events with at least three photons collected in pp collisions at $\sqrt{s}$ = 8 TeV with the ATLAS detector," *Eur. Phys. J. C*, Vol. 76, No. 4, 2016, pp. 210.

[7] Knapen, S., Lin, T., Lou, H. K., and Melia, T., "Searching for Axionlike Particles with Ultraperipheral Heavy-Ion Collisions," *Phys. Rev. Lett.*, Vol. 118, No. 17, 2017, pp. 171801.

[8] Jeans, D., Brient, J., and Reinhard, M., "GARLIC: GAmma Reconstruction at a LInear Collider experiment," *JINST*, Vol. 7, 2012, pp. P06003.

[9] Weinberg, S., "The Making of the standard model," *Eur. Phys. J. C*, Vol. 34, 2004, pp. 5–13.

[10] Higgs, P. W., "Broken Symmetries and the Masses of Gauge Bosons," *Phys. Rev. Lett.*, Vol. 13, 1964, pp. 508–509.

[11] Chatrchyan, S. et al., "Observation of a New Boson at a Mass of 125 GeV with the CMS Experiment at the LHC," *Phys. Lett. B*, Vol. 716, 2012, pp. 30–61.

[12] Aad, G. et al., "Observation of a new particle in the search for the Standard Model Higgs boson with the ATLAS detector at the LHC," *Phys. Lett. B*, Vol. 716, 2012, pp. 1–29.

[13] Ellis, J., Gaillard, M. K., and Nanopoulos, D. V., *A Historical Profile of the Higgs Boson*, 2016, pp. 255–274.

[14] Hasert, F., Kabe, S., Krenz, W., Von Krogh, J., Lanske, D., Morfin, J., Schultze, K., Weerts, H., Bertrand-Coremans, G., Sacton, J., Van Doninck, W., Vilain, P., Camerini, U., Cundy, D., Baldi, R., Danilchenko, I., Fry, W., Haidt, D., Natali, S., Musset, P., Osculati, B., Palmer, R., Pattison, J., Perkins, D., Pullia, A., Rousset, A., Venus, W., Wachsmuth, H., Brisson, V., Degrange, B., Haguenauer, M., Kluberg, L., Nguyen-Khac, U., Petiau, P., Belotti, E., Bonetti, S., Cavalli, D., Conta, C., Fiorini, E., Rollier, M., Aubert, B., Blum, D., Chounet, L., Heusse, P., Lagarrigue, A., Lutz, A., Orkin-Lecourtois, A., Vialle, J., Bullock, F., Esten, M., Jones, T., McKenzie, J., Michette, A., Myatt, G., and Scott, W., "Observation of neutrino-like interactions without muon or electron in the gargamelle neutrino experiment," *Physics Letters B*, Vol. 46, No. 1, 1973, pp. 138–140.

[15] et al., G. A., "Experimental observation of isolated large transverse energy electrons with associated missing energy at s=540 GeV," *Physics Letters B*, Vol. 122, No. 1, 1983, pp. 103–116.

[16] et al., M. B., "Observation of single isolated electrons of high transverse momentum in events with missing transverse energy at the CERN pp collider," *Physics Letters B*, Vol. 122, No. 5, 1983, pp. 476–485.

[17] Lee, B. W., Quigg, C., and Thacker, H. B., "Weak Interactions at Very High-Energies: The Role of the Higgs Boson Mass," *Phys. Rev. D*, Vol. 16, 1977, pp. 1519.

[18] Aaboud, M. et al., "Observation of electroweak production of a same-sign W boson pair in association with two jets in pp collisions at $\sqrt{s} = 13$ TeV with the ATLAS detector," *Phys. Rev. Lett.*, Vol. 123, No. 16, 2019, pp. 161801.

[19] Sirunyan, A. M. et al., "Observation of electroweak production of same-sign W boson pairs in the two jet and two same-sign lepton final state in proton-proton collisions at $\sqrt{s} = 13$ TeV," *Phys. Rev. Lett.*, Vol. 120, No. 8, 2018, pp. 081801.

[20] Sirunyan, A. M. et al., "Measurements of production cross sections of polarized same-sign W boson pairs in association with two jets in proton-proton collisions at $\sqrt{s} = 13$ TeV," *Phys. Lett. B*, Vol. 812, 2021, pp. 136018.

[21] Buarque, D. et al., "Vector Boson Scattering Processes: Status and Prospects," 6 2021.

[22] Chetyrkin, K. G., Kniehl, B. A., and Steinhauser, M., "Decoupling relations to O (alpha-s**3) and their connection to low-energy theorems," *Nucl. Phys. B*, Vol. 510, 1998, pp. 61–87.

[23] Schroder, Y. and Steinhauser, M., "Four-loop decoupling relations for the strong coupling," *JHEP*, Vol. 01, 2006, pp. 051.

[24] Sirunyan, A. M. et al., "Search for invisible decays of a Higgs boson produced through vector boson fusion in proton-proton collisions at $\sqrt{s} = 13$ TeV," *Phys. Lett. B*, Vol. 793, 2019, pp. 520–551.

[25] Garrett, K. and Duda, G., "Dark Matter: A Primer," *Adv. Astron.*, Vol. 2011, 2011, pp. 968283.

[26] SLAC Summer Institute on Particle Physics, *Dark Matter Candidates*, August 2004.

[27] Moore, B., "An Upper limit to the mass of black holes in the halo of our galaxy," *Astrophys. J. Lett.*, Vol. 413, 1993, pp. L93.

[28] Roszkowski, L., Sessolo, E. M., and Trojanowski, S., "WIMP dark matter candidates and searches—current status and future prospects," *Reports on Progress in Physics*, Vol. 81, No. 6, may 2018, pp. 066201.

[29] Weinberg, S., "A New Light Boson?" *Phys. Rev. Lett.*, Vol. 40, Jan 1978, pp. 223–226.

[30] di Wu and, D., "A Brief Introduction to the Strong CP Problem," September 1991.

[31] Boyarsky, A., Drewes, M., Lasserre, T., Mertens, S., and Ruchayskiy, O., "Sterile neutrino Dark Matter," *Prog. Part. Nucl. Phys.*, Vol. 104, 2019, pp. 1–45.

[32] Sakharov, A. D., "Violation of CP Invariance, C asymmetry, and baryon asymmetry of the universe," *Pisma Zh. Eksp. Teor. Fiz.*, Vol. 5, 1967, pp. 32–35.

[33] Riotto, A., "Theories of baryogenesis," *ICTP Summer School in High-Energy Physics and Cosmology*, 7 1998.

[34] Zyla, P. et al., "Review of Particle Physics," *PTEP*, Vol. 2020, No. 8, 2020, pp. 083C01.

[35] Asner, D. et al., "Averages of b-hadron, c-hadron, and τ-lepton properties," 10 2010.

[36] Abe, K. et al., "Constraint on the matter–antimatter symmetry-violating phase in neutrino oscillations," *Nature*, Vol. 580, No. 7803, 2020, pp. 339–344, [Erratum: Nature 583, E16 (2020)].

[37] Ahmad, Q. R. et al., "Direct evidence for neutrino flavor transformation from neutral current interactions in the Sudbury Neutrino Observatory," *Phys. Rev. Lett.*, Vol. 89, 2002, pp. 011301.

[38] Gell-Mann, M., Ramond, P., and Slansky, R., "Complex Spinors and Unified Theories," *Conf. Proc. C*, Vol. 790927, 1979, pp. 315–321.

[39] Ligeti, Z., "Flavor Constraints on New Physics," *PoS*, Vol. LeptonPhoton2015, 2016, pp. 031.

[40] Drees, M., Godbole, R., and Roy, P., *Theory and phenomenology of sparticles: An account of four-dimensional N=1 supersymmetry in high energy physics*, 2004.

[41] Baer, H., Barger, V., Salam, S., Sengupta, D., and Sinha, K., "Status of weak scale supersymmetry after LHC Run 2 and ton-scale noble liquid WIMP searches," *Eur. Phys. J. ST*, Vol. 229, No. 21, 2020, pp. 3085–3141.

[42] Feng, J. L., Grivaz, J.-F., and Nachtman, J., "Searches for Supersymmetry at High-Energy Colliders," *Rev. Mod. Phys.*, Vol. 82, 2010, pp. 699–727.

[43] Einhorn, M. B., Jones, D. R. T., and Veltman, M. J. G., "Heavy Particles and the rho Parameter in the Standard Model," *Nucl. Phys. B*, Vol. 191, 1981, pp. 146–172.

[44] López-Val, D. and Robens, T., "Δr and the W-boson mass in the singlet extension of the standard model," *Phys. Rev. D*, Vol. 90, 2014, pp. 114018.

[45] Gorghetto, M. and Villadoro, G., "Topological Susceptibility and QCD Axion Mass: QED and NNLO corrections," *JHEP*, Vol. 03, 2019, pp. 033.

[46] Cheng, H.-Y., "The Strong CP Problem Revisited," *Phys. Rept.*, Vol. 158, 1988, pp. 1.

[47] Dine, M., Fischler, W., and Srednicki, M., "A simple solution to the strong CP problem with a harmless axion," *Physics Letters B*, Vol. 104, No. 3, 1981, pp. 199–202.

[48] Kim, J. E., "Weak Interaction Singlet and Strong CP Invariance," *Phys. Rev. Lett.*, Vol. 43, 1979, pp. 103.

[49] Sheff, B., Steinberg, N., and Wells, J. D., "Higgs boson decays into narrow diphoton jets and their search strategies at the Large Hadron Collider," *Phys. Rev. D*, Vol. 104, No. 3, 2021, pp. 036009.

[50] Steinberg, N. and Wells, J. D., "Axion-Like Particles at the ILC Giga-Z," 1 2021.

[51] Steinberg, N., "Discovering Axion-Like Particles with Photon Fusion at the ILC," 8 2021.

[52] Sirunyan, A. M. et al., "Search for invisible decays of a Higgs boson produced through vector boson fusion in proton-proton collisions at $\sqrt{s} = 13$ TeV," *Phys. Lett. B*, Vol. 793, 2019, pp. 520–551.

[53] Aaboud, M. et al., "Measurements of Higgs boson properties in the diphoton decay channel with 36 fb^{-1} of pp collision data at $\sqrt{s} = 13$ TeV with the ATLAS detector," *Phys. Rev. D*, Vol. 98, 2018, pp. 052005.

[54] Belanger, G., Dumont, B., Ellwanger, U., Gunion, J., and Kraml, S., "Global fit to Higgs signal strengths and couplings and implications for extended Higgs sectors," *Phys. Rev. D*, Vol. 88, 2013, pp. 075008.

[55] Aad, G. et al., "Combined measurements of Higgs boson production and decay using up to 80 fb^{-1} of proton-proton collision data at $\sqrt{s} = 13$ TeV collected with the ATLAS experiment," *Phys. Rev. D*, Vol. 101, No. 1, 2020, pp. 012002.

[56] Aad, G. et al., "Measurements of the Higgs boson production and decay rates and constraints on its couplings from a combined ATLAS and CMS analysis of the LHC pp collision data at $\sqrt{s} = 7$ and 8 TeV," *JHEP*, Vol. 08, 2016, pp. 045.

[57] Curtin, D. et al., "Exotic decays of the 125 GeV Higgs boson," *Phys. Rev. D*, Vol. 90, No. 7, 2014, pp. 075004.

[58] Aad, G. et al., "A search for the dimuon decay of the Standard Model Higgs boson with the ATLAS detector," 7 2020.

[59] Aad, G. et al., "Combination of searches for Higgs boson pairs in pp collisions at $\sqrt{s}$ =13 TeV with the ATLAS detector," *Phys. Lett. B*, Vol. 800, 2020, pp. 135103.

[60] Dobrescu, B. A., Landsberg, G. L., and Matchev, K. T., "Higgs boson decays to CP odd scalars at the Tevatron and beyond," *Phys. Rev. D*, Vol. 63, 2001, pp. 075003.

[61] Draper, P. and McKeen, D., "Diphotons from Tetraphotons in the Decay of a 125 GeV Higgs at the LHC," *Phys. Rev. D*, Vol. 85, 2012, pp. 115023.

[62] Collaboration, A., "Search for new phenomena in events with at least three photons collected in pp collisions at $\sqrt{s}$ = 8 TeV with the ATLAS detector," *The European Physical Journal C*, Vol. 76, No. 4, April 2016, pp. 210, arXiv: 1509.05051.

[63] Chang, S., Fox, P. J., and Weiner, N., "Visible Cascade Higgs Decays to Four Photons at Hadron Colliders," *Phys. Rev. Lett.*, Vol. 98, 2007, pp. 111802.

[64] Ellis, S. D., Roy, T. S., and Scholtz, J., "Phenomenology of Photon-Jets," *Phys. Rev.*, Vol. D87, No. 1, 2013, pp. 014015.

[65] "Search for a Higgs boson decaying to four photons through light CP-odd scalar coupling using 7 TeV pp collision data taken with ATLAS detector at the LHC," 7 2012.

[66] Chawdhry, H. A., Czakon, M., Mitov, A., and Poncelet, R., "NNLO QCD corrections to three-photon production at the LHC," *Journal of High Energy Physics*, Vol. 2020, No. 2, Feb. 2020, pp. 57, arXiv: 1911.00479.

[67] Aaboud, M. et al., "A search for pairs of highly collimated photon-jets in pp collisions at $\sqrt{s}$ = 13 TeV with the ATLAS detector," *Phys. Rev. D*, Vol. 99, No. 1, 2019, pp. 012008.

[68] Collaboration, A., "Electron and photon performance measurements with the ATLAS detector using the 2015-2017 LHC proton-proton collision data," *Journal of Instrumentation*, Vol. 14, No. 12, Dec. 2019, pp. P12006–P12006, arXiv: 1908.00005.

[69] Robens, T. and Stefaniak, T., "Status of the Higgs Singlet Extension of the Standard Model after LHC Run 1," *Eur. Phys. J. C*, Vol. 75, 2015, pp. 104.

[70] Barger, V., Langacker, P., McCaskey, M., Ramsey-Musolf, M. J., and Shaughnessy, G., "LHC Phenomenology of an Extended Standard Model with a Real Scalar Singlet," *Phys. Rev. D*, Vol. 77, 2008, pp. 035005.

[71] Robens, T., Stefaniak, T., and Wittbrodt, J., "Two-real-scalar-singlet extension of the SM: LHC phenomenology and benchmark scenarios," *Eur. Phys. J. C*, Vol. 80, No. 2, 2020, pp. 151.

[72] Csaki, C., D'Agnolo, R. T., Geller, M., and Ismail, A., "Crunching Dilaton, Hidden Naturalness," 7 2020.

[73] Aaltonen, T. A. et al., "First Search for Exotic Z Boson Decays into Photons and Neutral Pions in Hadron Collisions," *Phys. Rev. Lett.*, Vol. 112, 2014, pp. 111803.

[74] Alwall, J., Frederix, R., Frixione, S., Hirschi, V., Maltoni, F., Mattelaer, O., Shao, H. S., Stelzer, T., Torrielli, P., and Zaro, M., "The automated computation of tree-level and next-to-leading order differential cross sections, and their matching to parton shower simulations," *JHEP*, Vol. 07, 2014, pp. 079.

[75] Sjostrand, T., Mrenna, S., and Skands, P. Z., "PYTHIA 6.4 Physics and Manual," *JHEP*, Vol. 05, 2006, pp. 026.

[76] Sjostrand, T., Mrenna, S., and Skands, P. Z., "A Brief Introduction to PYTHIA 8.1," *Comput. Phys. Commun.*, Vol. 178, 2008, pp. 852–867.

[77] de Favereau, J., Delaere, C., Demin, P., Giammanco, A., Lema

[78] Cacciari, M., Salam, G., and Soyez, G., "FastJet user manual," *Eur. Phys. J. C*, Vol. 72, No. 1896, 2012.

[79] Thaler, J. and Van Tilburg, K., "Identifying Boosted Objects with N-subjettiness," *JHEP*, Vol. 03, 2011, pp. 015.

[80] Chakraborty, A., Iyer, A. M., and Roy, T. S., "A Framework for Finding Anomalous Objects at the LHC," *Nuclear Physics B*, Vol. 932, July 2018, pp. 439–470, arXiv: 1707.07084.

[81] "Particle-Flow Event Reconstruction in CMS and Performance for Jets, Taus, and MET," 4 2009.

[82] Carena, M., Liu, Z., and Wang, Y., "Electroweak phase transition with spontaneous Z_2-breaking," *JHEP*, Vol. 08, 2020, pp. 107.

[83] Duffy, L. D. and van Bibber, K., "Axions as Dark Matter Particles," *New J. Phys.*, Vol. 11, 2009, pp. 105008.

[84] Athron, P. et al., "Status of the scalar singlet dark matter model," *Eur. Phys. J. C*, Vol. 77, No. 8, 2017, pp. 568.

[85] Svrcek, P. and Witten, E., "Axions In String Theory," *JHEP*, Vol. 06, 2006, pp. 051.

[86] Ringwald, A., "Axions and Axion-Like Particles," *49th Rencontres de Moriond on Electroweak Interactions and Unified Theories*, 2014, pp. 223–230.

[87] Beacham, J. et al., "Physics Beyond Colliders at CERN: Beyond the Standard Model Working Group Report," *J. Phys. G*, Vol. 47, No. 1, 2020, pp. 010501.

[88] Kim, J. E., "Light Pseudoscalars, Particle Physics and Cosmology," *Phys. Rept.*, Vol. 150, 1987, pp. 1–177.

[89] Bauer, M., Neubert, M., Renner, S., Schnubel, M., and Thamm, A., "The Low-Energy Effective Theory of Axions and ALPs," 12 2020.

[90] Chala, M., Guedes, G., Ramos, M., and Santiago, J., "Running in the ALPs," 12 2020.

[91] Graham, P. W., Irastorza, I. G., Lamoreaux, S. K., Lindner, A., and van Bibber, K. A., "Experimental Searches for the Axion and Axion-Like Particles," *Ann. Rev. Nucl. Part. Sci.*, Vol. 65, 2015, pp. 485–514.

[92] Powell, A. J., *The cosmology and astrophysics of axion-like particles*, Ph.D. thesis, Oxford U., 2016.

[93] Millea, M., Knox, L., and Fields, B., "New Bounds for Axions and Axion-Like Particles with keV-GeV Masses," *Phys. Rev. D*, Vol. 92, No. 2, 2015, pp. 023010.

[94] Feng, J. L., Galon, I., Kling, F., and Trojanowski, S., "Axionlike particles at FASER: The LHC as a photon beam dump," *Phys. Rev. D*, Vol. 98, No. 5, 2018, pp. 055021.

[95] Kowalczyk, E. and Blinov, N., "Searching for Axion-like Particles at DarkQuest," 10 2020.

[96] Abudinén, F. et al., "Search for Axion-Like Particles produced in e^+e^- collisions at Belle II," *Phys. Rev. Lett.*, Vol. 125, No. 16, 2020, pp. 161806.

[97] Bauer, M., Heiles, M., Neubert, M., and Thamm, A., "Axion-Like Particles at Future Colliders," *Eur. Phys. J. C*, Vol. 79, No. 1, 2019, pp. 74.

[98] Gershtein, Y., Knapen, S., and Redigolo, D., "Probing naturally light singlets with a displaced vertex trigger," 12 2020.

[99] Darmé, L., Giacchino, F., Nardi, E., and Raggi, M., "Invisible decays of axion-like particles: constraints and prospects," 12 2020.

[100] Glover, E. and Morgan, A., "Z boson decay into photons," *Phys. C - Particles and Fields*, Vol. 60, 1993, pp. 175–180.

[101] Acciarri, M. et al., "Search for anomalous Z –> gamma gamma gamma events at LEP," *Phys. Lett. B*, Vol. 345, 1995, pp. 609–616.

[102] Mimasu, K. and Sanz, V., "ALPs at Colliders," *JHEP*, Vol. 06, 2015, pp. 173.

[103] Ellis, S. D., Roy, T. S., and Scholtz, J., "Phenomenology of Photon-Jets," *Phys. Rev. D*, Vol. 87, No. 1, 2013, pp. 014015.

[104] Bambade, P. et al., "The International Linear Collider: A Global Project," 3 2019.

[105] Erler, J., Heinemeyer, S., Hollik, W., Weiglein, G., and Zerwas, P., "Physics impact of GigaZ," 5 2000, pp. 1389–1402.

[106] "The International Linear Collider Technical Design Report - Volume 2: Physics," 6 2013.

[107] Zhang, Y., Li, W., Duan, P., Song, M., and Li, G., "Electroweak radiative corrections to triple photon production at the ILC," *Phys. Lett. B*.

[108] Sjöstrand, T., Ask, S., Christiansen, J. R., Corke, R., Desai, N., Ilten, P., Mrenna, S., Prestel, S., Rasmussen, C. O., and Skands, P. Z., "An introduction to PYTHIA 8.2," *Comput. Phys. Commun.*, Vol. 191, 2015, pp. 159–177.

[109] Żarnecki, A. F., "Generic ILC detector model for Delphes," August 2020.

[110] Flórez, A., Gurrola, A., Johns, W., Sheldon, P., Sheridan, E., Sinha, K., and Soubasis, B., "Probing axionlike particles with $\gamma\gamma$ final states from vector boson fusion processes at the LHC," *Phys. Rev. D*, Vol. 103, No. 9, 2021, pp. 095001.

[111] d'Enterria, D., "Collider constraints on axion-like particles," *Workshop on Feebly Interacting Particles*, 2 2021.

[112] Baldenegro, C., Fichet, S., von Gersdorff, G., and Royon, C., "Searching for axion-like particles with proton tagging at the LHC," *JHEP*, Vol. 06, 2018, pp. 131.

[113] Budnev, V. M., Ginzburg, I. F., Meledin, G. V., and Serbo, V. G., "The Two photon particle production mechanism. Physical problems. Applications. Equivalent photon approximation," *Phys. Rept.*, Vol. 15, 1975, pp. 181–281.

[114] Alwall, J., Frederix, R., Frixione, S., Hirschi, V., Maltoni, F., Mattelaer, O., Shao, H. S., Stelzer, T., Torrielli, P., and Zaro, M., "The automated computation of tree-level and next-to-leading order differential cross sections, and their matching to parton shower simulations," *JHEP*, Vol. 07, 2014, pp. 079.

[115] Philipsen, O., "W W gamma couplings from single W production in polarized e+ e- collisions," *Z. Phys. C*, Vol. 54, 1992, pp. 643–652.

[116] de Favereau, J., Delaere, C., Demin, P., Giammanco, A., Lema

[117] Aad, G. et al., "Observation of light-by-light scattering in ultraperipheral Pb+Pb collisions with the ATLAS detector," *Phys. Rev. Lett.*, Vol. 123, No. 5, 2019, pp. 052001.

[118] Hirschi, V. and Mattelaer, O., "Automated event generation for loop-induced processes," *JHEP*, Vol. 10, 2015, pp. 146.

[119] Bhattiprolu, P. N., Martin, S. P., and Wells, J. D., "Criteria for projected discovery and exclusion sensitivities of counting experiments," *Eur. Phys. J. C*, Vol. 81, No. 2, 2021, pp. 123.

[120] Press, W. H., Flannery, B. P., Teukolsky, S. A., and Vetterling, W. T., *Numerical Recipes in Fortran 77: The Art of Scientific Computing 2nd Edition*, Cambridge University Press, 1992.

[121] Alloul, A., Christensen, N. D., Degrande, C., Duhr, C., and Fuks, B., "FeynRules 2.0 - A complete toolbox for tree-level phenomenology," *Comput. Phys. Commun.*, Vol. 185, 2014, pp. 2250–2300.

[122] Shtabovenko, V., Mertig, R., and Orellana, F., "FeynCalc 9.3: New features and improvements," *Comput. Phys. Commun.*, Vol. 256, 2020, pp. 107478.

[123] Peskin, M. E. and Schroeder, D. V., *An Introduction to quantum field theory*, Addison-Wesley, Reading, USA, 1995.